Research Square

Preprints are preliminary reports that have not undergone peer review.
They should not be considered conclusive, used to inform clinical practice,
or referenced by the media as validated information.

Serotonin reuptake inhibitors attenuate cardiac fibrosis in HFpEF by inhibiting the SERT-Hic5 pathway

Mingyang Zhao

zhaomingyang128@163.com

Peking University Health Science Center https://orcid.org/0009-0008-3243-8679

Article

Keywords: HFpEF, cardiac fibrosis, SSRI, serotonin transporter (SERT), Hic5

Posted Date: November 6th, 2026

DOI: https://doi.org/10.21203/rs.3.rs-11425226/v1

License: This work is licensed under a Creative Commons Attribution 4.0 International License.
Read Full License

Additional Declarations: There is **NO** Competing Interest.

Serotonin reuptake inhibitors attenuate cardiac fibrosis in HFpEF by inhibiting the SERT-Hic5 pathway

Mingyang Zhao[1#], Geng Bai[3#], Tao Shen[4], Xin Wang[1], Feifei Jin[2], Songtao Jiang[2], Junhui Zhao[1], Minghong Leng[1], Fenghe Yang[1], Meng Guo[3], Wanting Wang[1], Yuxin Zhang[1], Shi Jia[1], Jian Liu[3], Jingjing Ye[2*], Ming Zheng[1*]

[1]*Department of Physiology and Pathophysiology, School of Basic Medical Sciences, Peking University Health Science Center, and State Key Laboratory of Vascular Homeostasis and Remodeling, Peking University, Beijing 100191, P.R. China.*

[2]*Trauma Treatment Center, Peking University People's Hospital; Key Laboratory of Trauma Treatment and Neural Regeneration (Peking University), National Center for Trauma Medicine; Beijing 100044, P.R. China.*

[3]*Department of Cardiology, Peking University People's Hospital, Beijing, China.*

[4] *Department of Cardiology, Beijing Hospital, National Center of Gerontology, Institute of Geriatric Medicine, Chinese Academy of Medical Sciences & Peking Union Medical College, Beijing 100730, China.*

[#]*These authors contribute equally as co-first authors.*

[*]*Corresponding authors.*

Address Correspondence to:

Ming Zheng, M.D., Ph.D.

Department of Physiology and Pathophysiology, Health Science Center, Peking University, Beijing 100191, China

Tel.: 86-10-8280-5817, Fax: 86-10-8280-2403, E-Mail: zhengm@bjmu.edu.cn

Or to:

Jingjing Ye, M.D., Ph.D.

Trauma Treatment Center, National Center for Trauma Medicine, Peking University People's Hospital, Beijing 100044, China

Tel.: 86-10-8649-1490, E-Mail: yejingjing@pkuph.edu.cn

Funding Information

This work was supported by grants from the National Natural Science Foundation of China (32371242, 82572864, 31800974, 81873457 and 82470395), the National Key Research and Development Program of China (2020YFA0803802), Beijing Municipal Natural Science Foundation (7222193) and Beijing Tongzhou District Science and Technology Innovation Talent Outstanding Youth Project (JCQN2024006).

Acknowledgments

We are grateful to Prof. Yangpo Cao from Southern University of Science and Technology for sharing AAV9 packaging technology and plasmid vectors. We are also grateful to Qiang Shen, Lihua An of the Bioimaging and Analysis Laboratory from Peking University Health Science Center for technology support.

Abstract

HFpEF lacks therapies that directly reverse cardiac fibrosis. We used cMAP screening to identify SSRIs as candidate agents to reverse cardiac remodeling. In two independent clinical cohorts, SSRI exposure was associated with improved diastolic function, attenuated remodeling and reduced multiorgan dysfunction. Human myocardial biopsies linked SERT-Hic5 signaling to HFpEF severity. In a murine HFpEF model, fluvoxamine ameliorated diastolic dysfunction, hypertrophy and fibrosis by inhibiting fibroblast SERT. Our findings highlight the therapeutic potential of repurposing SSRIs targeting this fibroblast-specific pathogenic cascade for HFpEF and support further prospective investigation.

Keywords： HFpEF; cardiac fibrosis; SSRI; serotonin transporter (SERT); Hic5

Introduction

Heart failure with preserved ejection fraction (HFpEF) constitutes a growing global health burden, accounting for 15-50% of all heart failure cases[1]. Effective therapies remain limited, largely due to its poorly defined and diverse pathophysiology[2]. Emerging evidence from human myocardial and animal studies reveals a complex interplay of maladaptive pathways[3], including cardiomyocyte hypertrophy, progressive interstitial fibrosis, impaired cGMP–PKG signaling[4], systemic and myocardial inflammation[5, 6], endoplasmic reticulum (ER) stress with an impaired unfolded protein response (UPR)[7], metabolic inflexibility[8, 9], mitochondrial dysfunction[10,11], and activation of the DNA damage response[12]. Among these, progressive interstitial fibrosis stands out as a central pathological driver, which contributes directly to diastolic dysfunction and disease progression[13]. Therefore, targeting the molecular drivers of cardiac fibrosis represents a promising therapeutic strategy for HFpEF.

While targeting the molecular drivers of cardiac fibrosis is a rational strategy, the therapeutic armamentarium for HFpEF remains an area of active development. Recent guidelines have incorporated new agents based on large clinical trials[14]. For instance, sacubitril/valsartan (an angiotensin receptor-neprilysin inhibitor, ARNI) demonstrated a reduction in heart failure hospitalizations in certain patient subgroups[15], and evidence suggests it may modulate profibrotic signaling[16], as indicated by favorable changes in circulating extracellular matrix biomarkers such as TIMP-1 and sST2[17]. sacubitril/valsartan is reported to inhibit cardiac fibrosis and hypertrophy by

suppressing the TGF-β1/Smad3 signaling pathway[18], sFRP-1/Wnt/β-Catenin signaling pathway[19], neprilysin and AT1[20]. β-hydroxybutyrate, a ketone body produced by the liver, can alleviate mitochondrial hyperacetylation and inflammation in the pathogenesis of HFpEF[21]. Similarly, glucagon-like peptide-1 (GLP-1) receptor agonists like semaglutide have shown significant clinical benefit, particularly in obese HFpEF phenotypes[22]. However, direct evidence that drugs reverse established myocardial fibrosis at the tissue level—the core pathological substrate—remains limited. The urgent need for therapies that directly and potently target fibrotic remodeling underscores the importance of identifying novel druggable pathways.

To discover compounds that directly attenuate myocardial remodeling, we conducted a systematic drug screening and identified that selective serotonin reuptake inhibitors (SSRIs) suppress markers of cardiac hypertrophy and fibroblast activation. SSRIs primarily act by inhibiting the serotonin transporter (SERT, encoded by *SLC6A4*) [23], which mediates the reuptake of extracellular serotonin (5HT) into cells via a sodium-dependent symport mechanism[24]. Intracellular 5HT is degraded by monoamine oxidase A (MAO-A), a process that generates reactive oxygen species (ROS) like hydrogen peroxide (H_2O_2)[25]. Interestingly, H_2O_2 is a potent inducer of Hydrogen peroxide-Inducible Clone-5 (Hic5, encoded by *TGFB1I1*)[26]. Hic5, a downstream target of TGF-β and a transcriptional co-regulator, is critically involved in fibroblast activation by enhancing pro-fibrotic gene expression and inhibiting matrix degradation[27]. Studies have shown that Hic5 interacts with the C-terminus of SERT via its LIM domain,

facilitating SERT localization to the cell membrane[28, 29]. Hic5 can serve as a coactivator for P21[30] and c-fos[31], promoting downstream transcriptional responses such as extracellular matrix (ECM) production[32], enhancing the expression of ECM components including α-smooth muscle actin (αSMA), collagen (e.g., types I and III), and fibronectin, while inhibiting matrix metalloproteinases (MMPs), thereby reducing ECM degradation and contributing to tissue fibrosis[33, 34]. Prior evidence of an interaction between Hic5 and SERT[28] raises an interesting possibility: could a SERT-initiated signaling axis contribute to fibroblast activation in HFpEF? The direct role of SSRIs and this potential pathway in HFpEF remains unknown.

In this study, we integrate clinical data analysis, human myocardial tissue validation, animal models of HFpEF, and mechanistic cellular studies to investigate whether SSRIs confer benefits in HFpEF and the underlying mechanisms. We demonstrate that SSRI use is associated with improved diastolic function, attenuated cardiac remodeling, and reduced multi-organ dysfunction in HFpEF patients, and provide human myocardial tissue evidence linking SERT and Hic5 expression to cardiac function. In the well-established HFpEF mouse models, the SSRI fluvoxamine ameliorates diastolic dysfunction and cardiac fibrosis. Mechanistically, we find that SERT expression is specifically upregulated in cardiac fibroblasts, and the fibroblast-specific manipulation of SERT in vivo proves it can drive diastolic dysfunction and fibrosis via the Hic5-dependent pathway. Furthermore, we delineate the SERT/MAO-A/ROS/Hic5 signaling axis and show that SSRIs exert their benefits by inhibiting this

cascade, thereby suppressing fibroblast activation. Our findings reveal a novel pathogenic mechanism in HFpEF and identify the SSRIs' target, SERT, as a key regulator of fibrotic signaling, highlighting the therapeutic potential of regulating this pathway.

Materials and Methods

Patient Samples and clinical data

Samples of myocardial biopsy were obtained and conducted following guidelines of The Ethics Committee of the Peking University People's Hospital (Ethics Number 2020PHB373–01 and 2025PHB177-001) and Beijing Hospital (Ethics Number 2018BJYYEC-170-03). To investigate the relationship between SSRIs and HFpEF, a retrospective study was conducted. Patients were diagnosed with HFpEF according to the 2021 ESC Guidelines, which require the fulfillment of all three following criteria: 1) LVEF ≥50%; 2) Presence of signs and symptoms of heart failure; and 3) presence of at least one of the following conditions: cardiac structural abnormalities, left ventricular diastolic dysfunction (LVDD), or evidence of filling pressure. Cardiac structural abnormalities included left atrial diameter (LAD) >40 mm for males or >38 mm for females, a left ventricular mass index (LVMI) ≥115 g/m² for males or ≥95 g/m² for females, and a Relative Wall Thickness (RWT) >0.42. LVDD included E/e' ratio at rest >9, Filling pressures defined as BNP >35 pg/mL in sinus rhythm or >105 pg/mL in atrial fibrillation. The SSRIs analyzed in this study included fluoxetine, paroxetine, fluvoxamine, citalopram/ escitalopram. Age, sex, Body Mass Index (BMI), baseline comorbidities, and medication use between patients prescribed SSRI were compared. The multiple imputation (MICE) was applied to handle missing data. To account for non-randomized treatment assignment and indication bias, inverse probability of treatment weighting (IPTW) was applied. Stabilized IPTW weights were trimmed at the 95th percentile to mitigate the influence of extreme values. Baseline covariate balance was assessed using standardized mean differences (SMD), with a threshold of < 0.1 indicating optimal balance. Outcome analyses for continuous variables were

conducted using IPTW-weighted generalized linear models (GLMs) with a Gamma distribution and a log-link function. To further establish a doubly robust estimation approach, multivariable adjustment incorporating all baseline covariates was applied to compute adjusted ratios of means and 95% confidence intervals (CIs). Detailed clinical characteristics and mRNA expression data for the myocardial biopsy samples are provided in Table S1.

Data Analysis of Patients from the MIMIC IV Database

Patients with heart failure (HF) were initially identified from hospitalization records using International Classification of Diseases (ICD 9/10) codes. To accurately distinguish heart failure with preserved ejection fraction (HFpEF), the researchers extracted left ventricular ejection fraction (LVEF) values from unstructured text in discharge summaries, classifying cases with an LVEF of $\geqslant 50\%$ as HFpEF. The exposure was defined as in-hospital use of any selective serotonin reuptake inhibitor (SSRI), identified via prescription records for Sertraline, citalopram, escitalopram, fluoxetine, paroxetine, or fluvoxamine. Patients prescribed at least one SSRI during admission were classified as SSRI users. The following were excluded: Records with implausible LVEF values (>100%); Patients aged <18 or >90 years; Patients with missing key demographic data. Extracted variables included: Age, sex, Body Mass Index (BMI), baseline comorbidities, medication use, and Sequential Organ Failure Assessment (SOFA) score (admission and discharge). Outcomes included Primary mortality (All-cause mortality) and SOFA score in the discharge (total and cardiovascular). Baseline variables with >30% missingness (excluding outcomes) were

excluded. For missing data, we employed a non-parametric imputation method based on MICE. To account for non-randomized treatment assignment and indication bias, whilst maintaining consistency in our statistical approach, we adopted the same statistical strategy.

Experimental Animals and HFpEF Model

All animal procedures were approved by the Institutional Animal Care and Use Committee of Peking University Health Science Center. Male C57BL/6J mice (8-12 weeks of age) were used to avoid the potential confounding effects of estrogen fluctuations in females, consistent with established HFpEF modeling approaches[35]. Mice were housed under a 12-hour light/dark cycle at 23±3°C. To establish the HFpEF model, male mice were randomly assigned to receive a high-fat diet with L-NAME (0.8 g/L in drinking water) for 8 weeks. Control (wild-type) mice received a standard diet. All experimental operations and analyses were performed in a blinded manner.

Cell culture of cardiac fibroblasts and cardiomyocytes

Primary neonatal rat cardiac fibroblasts (NRCFs) were isolated from 1- to 2-day-old Sprague-Dawley rats. Ventricles were digested in HBSS containing 0.1% trypsin and 0.05% type II collagenase. The dissociated cells were collected by centrifugation, resuspended, and pre-plated for 2 hours, and the supernatant containing cardiomyocytes was subsequently removed to purify fibroblasts. Cardiac fibroblasts were cultured with DMEM nutrient medium containing 15% fetal bovine serum (FBS) (HyClone, USA) 48 hours. Then the cells were digested and passaged. The second passage cells cultured

to 70%-80% confluence was used for adenovirus transfection.

Adult male mouse cardiomyocytes and cardiac fibroblasts were isolated via Langendorff perfusion as previously described[36]. Briefly, hearts were perfused with a calcium-free solution followed by a collagenase-containing solution for 25-30 minutes. The digested left ventricular tissue was minced, triturated, and filtered through a 200-μm mesh. Cardiomyocytes were collected by natural sedimentation, while the supernatant was centrifuged to obtain fibroblasts which were isolated by 2-hour adherence plating.

Virus Construction

The full-length coding sequences of human *SLC6A4* (SERT) and *TGFB1I1* (Hic5) were amplified by PCR. The primer sequences were as follows: *SLC6A4* forward, 5'-GAGACGACGCCCTTGAATTCT-3' and reverse, 5'-TCAAGCGGATGTCCCCACA-3'; *TGFB1I1* forward, 5'-GAGGACCTGGATGCCCTGC-3' and reverse, 5'-TCAGCCGAAGAGCTTCAGGA-3'. The amplified products were cloned into the pENTR/TEV/D-TOPO vector and subsequently recombined with the pAd/CMV/V5-DEST vector to generate adenoviruses (Ad-SERT, Ad-HIC5). For knockdown, shRNA sequences (sh*Slc6a4*: GUCCAGCAUCUUGGUCAUCUUUCAAGAGAAGATGACCAAGATGCUGGA; sh*Tgfb1i1*: TCGAGGGACCAATCTGAAGACAAGCTCGAGCTTGTCTTCAGATTGGTCCT

TTTTTA) were cloned into the pENTR/U6 vector and recombined into the pBLOCK-iT-DEST vector to produce shRNA-encoding adenoviruses.

For in vivo studies, the cDNAs and shRNAs were packaged into adeno-associated virus serotype 9 (AAV9)- ZsGreen vectors. To achieve cardiac fibroblast-specific expression, vectors were driven by the Postn promoter, generating AAV9-Postn-SERT, AAV9-Postn-HIC5, AAV9-Postn-sh*Slc6a4*, and AAV9-Postn-sh*Tgfb1i1*. Control vectors included AAV9-Postn-LacZ and AAV9-Postn-scRNA. Mice received an intravenous injection of 2×10^{11} vector genomes of the above AAV9 virus, separately. Transduction efficiency and specificity were confirmed by Western blot and confocal microscopy of heart tissues. For the functional epistasis experiments, mice received AAV9-Postn-sh*Slc6a4* or AAV9-Postn-scRNA, followed by daily intraperitoneal injection of fluvoxamine (10 mg/kg/d) or vehicle for 4 weeks.

Echocardiography

Transthoracic echocardiography was performed using a Vevo770 system (Visual Sonics, Toronto, Ontario, Canada) under light anesthesia (1.2% isoflurane). Two-dimensional, B-mode, M-mode, pulsed-wave Doppler, and tissue Doppler images were acquired. Parameters measured included ejection fraction (EF), fractional shortening (FS), left ventricular posterior wall thickness at end-diastole (LVPWd), left ventricular internal diastolic (LVIDd), trans-mitral flow velocities (E, A), E/A ratio, early diastolic mitral annular velocity (e'), E/e' ratio, isovolumic relaxation time (IVRT), and deceleration time (DT). Analyses were based on three consecutive cardiac cycles.

Histological Analysis

Freshly isolated heart samples were fixed in 4% paraformaldehyde, paraffin-embedded, and sectioned. Sections were stained with hematoxylin and eosin (H&E) for general morphology and with Masson's trichrome staining for collagen deposition. Fibrosis was quantified as the percentage of blue-stained area relative to the total myocardial area using Image ProPlus 6.0 software. Images were captured on the NDP.view2 imaging workstation.

Western Blotting and In-Cell Western Assay

Protein expression was assessed by conventional Western blotting or In-Cell Western assay. For Western blotting, proteins were extracted from ventricular tissues or cultured cells using RIPA buffer (Applygen, China), separated by SDS-PAGE, and transferred to PVDF membranes (Merck Millipore, Germany). Membranes were blocked and incubated overnight at 4°C with primary antibodies against ANP, αSMA, fibronectin (FN, Abcam), SERT, Hic5, or α-tubulin (Santa Cruz Biotechnology), followed by incubation with HRP-conjugated secondary antibodies (goat anti-rabbit or anti-mouse IgG; Biodragon or Abbkine, USA) and ECL detection.

For the In-Cell Western assay, cells seeded in 96-well plates were fixed, permeabilized, and blocked after treatment. Primary antibodies against Anp, FN, and α-tubulin were incubated overnight at 4°C. After washing with PBS, fluorescent secondary antibodies (AB150113, AB150115 from Abcam) were incubated for 2 hours at room temperature. Fluorescence signals were measured at 488 nm emission wavelength.

RNA Sequencing and Quantitative RT-PCR

Total RNA was extracted from mouse cardiac fibroblasts or flash frozen mouse hearts using TRIzol reagent. RNA integrity and purity were assessed by Shanghai Majorbio Biopharm Technology Co.,Ltd (Shanghai, China) according the manufacturer's instructions. RNA quality was verified (OD260/280: 1.8–2.2; RIN ≥ 6.5). RNA sequencing libraries were prepared with the Illumina Stranded mRNA Prep Ligation kit and sequenced on a NovaSeq X Plus platform (2×150 bp).

Total RNA was extracted from rat neonatal cardiac fibroblasts using TRIzol reagent (Invitrogen, USA). RNA was reverse-transcribed to cDNA using the Transcriptor First Strand cDNA Synthesis kit (Thermo Fisher, USA). RT-PCR was performed using SYBR green fluorescence (Thermo Fisher, USA). The mRNA expression levels of target genes were normalized to *Gapdh* and calculated using the comparative CT method. The sequences of all primers used are listed.

	Forward primer (5'-3')	Reverse primer (5'-3')
Tgfb1i1	ATGTCACGGTTAGGGGCTC	GGCTTGCATACTGTGCTGTATAG
Col1a1	CTGGCGGTTCAGGTCCAAT	TTCCAGGCAATCCACGAGC
Col3a1	CAATGTAAAGAAGTCTCTGAAG	CAAACAGGGCCAATGTCCAC
Fn1	GCCGTTAGATGTGCAAGCTG	TGCTGAAGCTGAGAACTAGGC
Anp	ATGGGCTCCTTCTCCATCAC	GTGTTGGACACCGCACTGTA
P21	TCCTGGTGATGTCCGACCTGTTC	CAGAGTGCAAGACAGCGACAAGG
C-fos	TCTCTAGTGCCAACTTTATCCC	GAGATAGCTGCTCTACTTTGCC
Mmp1	CTTCCTGATGATGACGTTCAAG	GTCACACTTCTCTGGTGTTTTG

Mmp9	ACTCGGATTTCCAAGACGTG TGAAG	TCTGTCCATTGCTTGTGCCAT CTC
Acta2	CTGTGCTATGTCGCTCTGGA	ATAGGTGGTTTCGTGGATGC
Tgfb1	CCAGATCCTGTCCAAACTAA GG	CTCTTTAGCATAGTAGTCCG CT
Ctgf	GAAGCTGACCTGGAGGAAA A	ACTGGCAGAGTGGTGGTTCT
Gapdh	AAGAAGGTGGTGAAGCAG	TCATACCAGGAAATGAGC

Enzyme-Linked Immunosorbent Assay (ELISA)

Serum Bnp levels were measured using a commercial mouse Bnp sandwich ELISA kit (MEIMIAN) according to the manufacturer's instructions. Absorbance was measured at 450 nm.

Immunofluorescence

Cardiac fibroblasts or Mouse Embryonic Fibroblasts (MEFs) on Laser confocal petri dish were fixed, permeabilized, and blocked with 5% BSA. Samples were incubated with primary antibodies overnight at 4°C, followed by Alexa Fluor-conjugated secondary antibodies. Nuclei were stained with DAPI (Sigma-Aldrich). Images were acquired using a laser scanning confocal microscope (TCS SP5 II, Leica).

Reactive Oxygen Species (ROS) Measurement

Intracellular ROS levels were detected using the fluorescent probe DCFH-DA. Cells were incubated with 10 μM DCFH-DA for 20 minutes at 37°C. After washing, fluorescence was visualized by confocal microscopy or quantified using a microplate reader (excitation/emission: 488/525 nm).

5HT/Fluvoxamine Quantification by LC-MS/MS

Plasma 5HT levels were quantified using liquid chromatography-tandem mass spectrometry (LC-MS/MS). Samples were separated on a Dionex UltiMate 3000 system equipped with a C18 column (2.1 × 100 mm, 1.8 μm) at 40°C, using a gradient of 0.1% formic acid in water (mobile phase A) and 0.1% formic acid in acetonitrile (mobile phase B) at a flow rate of 0.3 mL/min. Mass spectrometric detection was performed on a triple quadrupole instrument in positive electrospray ionization mode, with 5HT quantified via multiple reaction monitoring (MRM) by tracking the transition m/z 177→160. Calibration curves were constructed from serially diluted standards, and analyte concentrations were determined by normalizing peak areas to the internal standard 5HT-d4.

For plasma fluvoxamine quantification, blood samples were collected at 30 min, 1 h, 2 h, 4 h, 8 h, and 24 h after the first intraperitoneal injection, with additional time points (36 h, 48 h, 72 h, 96 h) during once-daily dosing. Samples were centrifuged at 4°C and plasma was stored at -80°C until analysis. Fluvoxamine was extracted from plasma samples by protein precipitation, and quantified via MRM using a specific transition for fluvoxamine. Calibration curves were constructed from serially diluted standards, and analyte concentrations were determined by normalizing peak areas to an internal standard.

Statistical analyses

Statistical data were presented as mean ± SEM (standard error of mean). Statistical

analyses were performed using GraphPad Prism (version 9.0) and SAS. For samples with n≥6 per group, the Shapiro-Wilk normality test was first applied. For normally distributed data, unpaired two-tailed Student' s t test was used to compare two groups; one-way analysis of variance (ANOVA) followed by Dunnett' s post-hoc test was used to compare differences among >2 groups with one control group; two-way ANOVA followed by Bonferroni's post-hoc multi-comparison test was used for experiments involving two independent variables (e.g., treatment group and time), to assess the main effects of each factor and their interaction. For non-normally distributed or small sample size (n<6) data, the Mann Whitney U test was used for two groups, and Kruskal-Wallis H test followed by Dunnett' s post-hoc test or Dunn-Bonferroni was used for multiple groups. Log rank test was used for Kaplan-Meier curves. All of the statistical experiments were repeated at least three times independently. P<0.05 was considered statistically significant. The representative image was selected from one of the repeated experiments that best matched the mean value.

Results

cMAP-based screening identifies SSRIs and clinical data suggest that SSRIs ameliorate pathological cardiac remodeling and multi-organ dysfunction in HFpEF

Pathological myocardial remodeling, characterized by hypertrophy and fibrosis, is a hallmark of HFpEF[37]. Histological analysis of human endomyocardial biopsy samples using H&E and Masson's trichrome staining confirmed this myocardial remodeling in hearts from patients with HFpEF, as well as in those with HFrEF (Fig. 1A). To identify

potential compounds capable of ameliorating these pathological features, we screened the Connectivity Map (cMAP) database for agents predicted to counteract the transcriptional signatures from both fibrotic (28 days post-myocardial infarction) and hypertrophic (transverse aortic constriction, TAC) cardiac remodeling in mice (Fig. 1B). This approach yielded an intersection of 147 candidate compounds. To validate this finding, we selected clinically relevant compounds for further testing. Using an in-cell Western assay in isolated and cultured rat neonatal primary cardiomyocytes and fibroblasts, we evaluated the effects of 64 candidate drugs that have been clinically applied on key remodeling markers. Notably, among the 13 drugs with significant effects, four SSRIs—fluvoxamine maleate, vortioxetine, escitalopram oxalate, and paroxetine HCl—that were also among the cMAP-predicted hits, consistently suppressed the upregulation of the hypertrophic marker atrial natriuretic peptide (ANP) in cardiomyocytes and the fibrotic marker fibronectin (FN) in fibroblasts (Fig. 1C). This functional validation supported their potential role to mitigate adverse cardiac remodeling. Given the widespread clinical use of SSRIs and the high prevalence of comorbid depression in heart failure, we examined the association between SSRI use and cardiac function in HFpEF patients. To investigate this, we conducted a retrospective analysis of 730 HFpEF patients (median age 70 [IQR 62-77] years; 54.93% male) from Peking University People's Hospital (2022–2024) (Fig. 1D). Baseline characteristics stratified by SSRIs use are summarized in Table 1: Patients receiving SSRIs were more likely to be female, had a lower body mass index and prevalence of hyperlipidaemia, but higher rates of chronic kidney disease and coronary heart disease.

They were also less frequently treated with SGLT2 inhibitors (Table 1, Fig. 1E). To address these baseline imbalances, we applied inverse probability of treatment weighting (IPTW). After IPTW adjustment, SSRI use remained significantly associated with better cardiac structure and function parameters, including lower plasma BNP levels, reduced E/e' ratio, smaller left atrial diameter (LAD), and lower left ventricular mass index (LVMI) (Fig. S1A). Following comprehensive multivariable adjustment using gamma generalized linear models, SSRI treatment remained independently associated with reduced BNP (ratio of means 0.664, 95% CI 0.532 - 0.828; $P = 0.0003$), lower E/e' ratio (ratio of means 0.923, 95% CI 0.857 - 0.994; $P = 0.0352$), and decreased LVMI (ratio of means 0.931, 95% CI 0.884 - 0.981; $P = 0.0076$) (Fig. 1E, Table 2).

To independently validate the clinical association and explore outcomes in a high-acuity setting, we analyzed data from the MIMIC-IV database, focusing on critically ill patients with HFpEF. A total of 1,089 patients with HFpEF were included (median age 74 [IQR 65–81] years; 47.9% male) (Fig. 1F-left). Baseline characteristics showed that patients receiving SSRI treatment were more likely to be female, younger, and had a higher BMI (Table 3). Their admission SOFA scores were also frequently lower, suggesting better baseline organ function (Fig. 1F-middle). To address these imbalances, we also applied the IPTW, which successfully balanced all baseline covariates (Fig. S1B). After IPTW, multivariable gamma generalized linear models revealed that SSRI use was independently associated with a lower SOFA score at discharge (ratio of means 0.818, 95% CI 0.746 - 0.898; $P<0.001$) (Fig. 1F-right, Table 4). Given that SOFA score

362 is a well-established predictor and outcome measure of mortality in critical illness[38],
363 this association suggests a potential survival benefit. Consistent with this trend of
364 improved multi-organ function, SSRI use was associated with numerically lower all-
365 cause mortality and a lower cardiovascular SOFA score at discharge, although neither
366 association reached statistical significance (Fig.1F-right). Together, analysis of these
367 independent, high-acuity ICU cohort supports the association between SSRIs and
368 improved clinical status in HFpEF, and further implies benefits that may extend beyond
369 the heart to improve systemic organ function.

370 **SSRI fluvoxamine ameliorates diastolic dysfunction and cardiac remodeling in the**
371 **HFpEF mouse model**

372 Based on these clinical correlations and the above screening which pinpointed
373 fluvoxamine for its superior efficacy in lowering FN and ANP in cells (Fig 1C), we
374 selected this representative SSRI for direct functional validation in a well-established
375 "two-hit" HFpEF mouse model induced by HFD and L-NAME (Fig. 2A, S2B-G). Mice
376 were treated with fluvoxamine via intraperitoneal injection (10 mg/kg/d) under two
377 conditions: as a prophylactic treatment throughout the 8-week induction phase, or as a
378 therapeutic intervention during weeks 8-12 following established HFpEF (Fig. 2A).
379 This dosage is effective in mouse models of related conditions[39, 40]. We also monitored
380 the plasma drug concentration and found that continuous administration could maintain
381 the drug concentration at a relatively stable level (Fig. S2A). Treatment at this dose
382 showed no significant hepatic or renal toxicity (Fig. S3C). Doppler echocardiography

revealed HFpEF mice developed diastolic dysfunction, characterized by increased E/A and E/e' ratios, while left ventricular ejection fraction (EF) or fractional shortening (FS) were preserved (Fig. 2B, S3A). Both preventive and therapeutic administration of fluvoxamine significantly ameliorated the diastolic function, as evidenced by reductions in E/A and E/e' ratios compared to the untreated HFpEF group (Fig. 2B). Furthermore, fluvoxamine treatment significantly attenuated the pathological increase in both the heart weight to tibia length (HW/TL) ratio and serum BNP levels induced by HFpEF mice, without affecting these parameters in control mice (Fig. 2C). Histological analysis via HE and Masson's trichrome staining further showed that fluvoxamine reduced cardiac collagen deposition (Fig. 2D, S3B). Consistent with the functional and structural improvements, western blot analysis of heart tissue confirmed that fluvoxamine treatment effectively suppressed the upregulation of the fibrotic markers FN and α-smooth muscle actin (αSMA) (Fig. 2E). Collectively, these findings demonstrate that SSRI fluvoxamine can ameliorate diastolic dysfunction, suppress hypertrophy, and inhibit cardiac fibrosis in HFpEF.

The SSRI target SERT is upregulated in HFpEF and promotes cardiac fibroblast activation

Since SSRIs exert their effects by inhibiting the serotonin transporter (SERT), we want to investigate the specific role of SERT in HFpEF. To validate the clinical relevance of our findings in human cardiac tissue, we analyzed myocardial biopsy samples from 11 patients across two centers (control n=3, HFpEF n=4, HFrEF n=4; Table S1). To our

knowledge, this is the first human tissue-level evidence linking SERT expression to cardiac function in HFpEF. SLC6A4 mRNA levels were upregulated in HFpEF samples, showing an approximately 3.31-fold increase compared with non-failing controls (Fig 3A). SLC6A4 mRNA level correlated positively with E/e' (Spearman $r_s = 0.69$, $p = 0.019$), indicating that higher SERT expression is associated with more severe diastolic dysfunction (Fig. 3B). No significant correlation was observed between SERT expression and LVEF or E/A ratio (Fig. 3B). In our mouse HFpEF model, western blot analysis and immunofluorescence staining revealed a significant upregulation of SERT protein in whole-heart tissues from HFpEF mice compared to control mice (Fig. 3C). To determine the cellular source of this increase, we isolated primary cardiac fibroblasts (CFs) and cardiomyocytes (CMs), and found that SERT upregulation was observed specifically in CFs, with no significant change in CMs. Quantitatively, SERT expression was increased by 1.93-fold in CFs compared to controls, whereas only a 1.19-fold change was detected in CMs (Fig.3C), suggesting a fibroblast-specific role for SERT in HFpEF pathogenesis. Consistent with this, *in vitro* stimulation of primary CFs with TGF-β, a classic pro-fibrotic stimulus[41], significantly increased SERT protein levels (Fig. 3D). We then performed gain- and loss-of-function experiments to identify role of SERT in fibroblast activation. Overexpression of SERT in primary CFs was sufficient to upregulate the fibrotic markers, including FN and alpha-smooth muscle actin (αSMA) (Fig. 3E). Conversely, pharmacological inhibition of SERT with 10 μM fluvoxamine effectively suppressed TGFβ-induced upregulation of FN and αSMA (Fig. 3F). These results identify SERT as a key regulator of cardiac fibroblast activation.

Fibroblast-specific SERT overexpression impairs, whereas its knockdown ameliorates, diastolic dysfunction in HFpEF mouse models

We further employed the AAV9 driven by the Postn promoter (AAV9-Postn) to assess the functional consequence of fibroblast-specific SERT modulation *in vivo.* C57BL/6J mice received tail vein injections of either the control AAV9-Postn-LacZ virus, AAV9-Postn-SERT to overexpress SERT, or AAV9-Postn-SERT combined with daily intraperitoneal administration of SERT inhibitor fluvoxamine (10 mg/kg/d) for 4 weeks (Fig. 4A, S4A). Echocardiography showed no significant differences in systolic function among the three groups (Fig. S4B). However, fibroblasts-specific SERT overexpression significantly impaired diastolic function, as indicated by increased E/A and E/e' ratios compared with the control group, which was effectively reversed by concurrent fluvoxamine treatment (Fig. 4B). Consistently, SERT overexpression induced significant cardiac interstitial fibrosis, characterized by elevated protein levels of FN and αSMA and increased collagen deposition area of Masson's trichrome staining, which were also attenuated by fluvoxamine (Fig. 4C, S4C). We next evaluated the therapeutic potential of SERT knockdown in established HFpEF. Mice were first subjected to a "two-hit" HFpEF induction protocol (HFD + 0.8 g/L L-NAME) for 4 weeks and then received tail vein injections of either AAV9-Postn-sh*Slc6a4* to knockdown SERT or a AAV9-Postn-scRNA control virus (Fig. 4D, S4D). Echocardiographic assessment at week 8 revealed that fibroblast-specific SERT knockdown improved diastolic function, as evidenced by a 21.57 reduction in E/e' ratio

and a decrease of 1.877 in the E/A ratio compared to the HFpEF control group (Fig. 4E). Furthermore, this intervention also counteracted the cardiac fibrosis and hypertrophy induced by HFpEF, as shown by decreased fibrotic marker expression, collagen deposition and serum BNP level (Fig. 4F, S4F-G). Together, these results demonstrate that SERT is a critical regulator of diastolic function and cardiac fibrosis during HFpEF. SERT upregulation promotes diastolic dysfunction, while its inhibition or knockdown ameliorates these pathological features, highlighting SERT as a potential therapeutic target.

SERT drives fibroblast activation via upregulation of Hic5

To elucidate the mechanism by which SERT drives fibroblast activation, we performed transcriptomic analysis on SERT-overexpressing fibroblasts. Intersection of differentially expressed genes with known factors in TGF-β-induced fibrosis identified Transforming Growth Factor Beta 1 Induced Transcript 1, also known as Hydrogen Peroxide Inducible Clone 5 (Hic5), as a candidate mediator (Fig. 5A). We validated that Hic5 expression was upregulated by SERT overexpression and TGF-β stimulated fibroblasts *in vitro* (Fig. 5B) and in the hearts of mice with fibroblast-specific SERT overexpression *in vivo* (Fig. 5C). To further corroborate this finding in human disease, we analyzed TGFB1I1 (Hic5) mRNA levels in myocardial biopsies and found that TGFB1I1 was upregulated in HFpEF samples compared with HFrEF, and its expression correlated positively with LVEF (Fig. 5D), providing human tissue-level evidence linking Hic5 to cardiac function in HFpEF. No significant correlation was observed

between Hic5 expression and E/e' or E/A ratio. In HFpEF mouse hearts, Hic5 was significantly elevated with SERT (Fig. 5E up). Functionally, Hic5 overexpression in fibroblasts alone was sufficient to induce fibroblast activation, as indicated by increased FN and αSMA expression (Fig. 5E down), while Hic5 knockdown attenuated the pro-fibrotic effects of SERT expression (Fig. 5F up), indicating that SERT promotes fibroblast activation through Hic5. Mechanistically, Hic5 is known to promote fibrosis by activating P21 and c-fos, so we examined these targets and their downstream pro-fibrotic pathway. RT-PCR showed that SERT overexpression significantly upregulated the expression of Hic5 targets (P21, c-fos) and downstream pro-fibrotic genes, all of which were entirely reversed by Hic5 knockdown (Fig. 5F down), confirming that SERT activates fibroblasts via Hic5-mediated transcription of fibrotic factors.

Fibroblast-specific Hic5 modulation is necessary and sufficient for HFpEF-like pathophysiology in vivo

To explore the role of Hic5 *in vivo*, we directly performed gain- and loss-of function studies. Fibroblast-specific overexpression of Hic5 in mouse hearts (Fig. 6A, S5A) was sufficient to recapitulate the HFpEF like phenotypes, including severe diastolic dysfunction (Fig. 6B, S5B) and cardiac fibrosis (Fig. 6C, S5C). Conversely, fibroblast-specific knockdown of Hic5 in a mouse model of HFpEF (Fig. 6D, S5D) improved diastolic function (Fig. 6E, S5E), as evidenced by reduced E/A and E/e’ ratios (E/A: from 3.93±0.21 in HFpEF mice to 2.01±0.41; for E/e’: from 44.4±11.1 to 25.8±10.0), and attenuated cardiac fibrosis as evidenced by decreased FN, αSMA and collagen deposition area of Masson’s trichrome staining (Fig. 6F, S5F). Collectively, these *in*

vivo data reveal Hic5 as an essential mediator of SERT-driven cardiac fibrosis in HFpEF.

SERT upregulates Hic5 through 5HT uptake and MAO-A-dependent ROS generation

Given that Hic5 (Hydrogen Peroxide Inducible Clone 5) is transcriptionally induced by hydrogen peroxide (H_2O_2) stimulation[26] (Fig. S6B), and that SERT-mediated 5HT uptake into cells leads to its degradation by monoamine oxidase A (MAO-A), a process that generates H_2O_2, we therefore investigated whether SERT promotes Hic5 expression via ROS generation. Indeed, overexpression of SERT in cardiac fibroblasts resulted in a 1.63-fold increase in intracellular ROS levels (Fig. 7A). Treatment with a ROS scavenger N-acetylcysteine (LNAC) suppressed both Hic5 upregulation and fibroblast activation (Fig. 7A, B), suggesting that SERT upregulates Hic5 via ROS. Next, we found that the MAO-A inhibitor clorgyline effectively reduced intracellular ROS, prevented Hic5 upregulation, and inhibited fibroblast activation induced by SERT overexpression. Critically, the suppressive effects of clorgyline were fully reversed by supplementation with exogenous H_2O_2 (Fig. 7C, D), indicating that SERT promotes ROS production through MAO-A-mediated 5HT degradation, leading to increased Hic5 expression and fibroblast activation. To confirm the necessity of 5HT in this pathway, we cultured fibroblasts in 5HT-depleted medium (using charcoal-stripped FBS) (Fig. 7E). Culturing fibroblasts in 5HT-depleted medium completely abolished the ability of SERT overexpression to increase ROS, upregulate Hic5, or induce fibrotic marker FN expression (Fig. 7E, F). Subsequent replenishment of 5HT restored ROS generation, Hic5 and FN expression (Fig. 7E, F). These results demonstrate that SERT-mediated 5HT uptake facilitates its degradation by MAO-A, leading to ROS generation,

512 which in turn upregulates Hic5 expression, ultimately driving cardiac fibroblast
513 activation and fibrosis. These results provide a potential mechanism for how SSRIs, by
514 inhibiting the initial step (SERT), may exert their anti-fibrotic effects in HFpEF.

515 **SSRIs attenuate cardiac fibrosis by inhibiting SERT-ROS-Hic5 axis**

516 Based on we identified pro-fibrotic SERT-ROS-Hic5 pathway, we next investigated
517 whether the therapeutic effects of SSRIs during HFpEF are mediated through the
518 inhibition of this specific axis. In fibroblasts overexpressing SERT, fluvoxamine
519 treatment effectively inhibited the SERT-induced increase in intracellular ROS levels
520 (Fig. 8A) and subsequently blocked the upregulation of Hic5 and fibrotic markers (Fig.
521 8A, B). We then investigated these findings *in vivo* using our HFpEF mouse model.
522 Compared to HFpEF controls, both preventive (weeks 1-8) and therapeutic (weeks 8-
523 12) administration of fluvoxamine significantly reduced the elevated ROS levels by
524 58.7% and 59.0%, respectively (Fig. 8B). At the protein level, preventive SSRI
525 treatment markedly attenuated the HFpEF-induced upregulation of both SERT and
526 Hic5 proteins. Notably, while therapeutic treatment robustly reduced SERT expression,
527 its effect on Hic5 was less pronounced (Fig. 8B, C), suggesting that early intervention
528 may be more effective in disrupting this pathogenic cascade. To unequivocally establish
529 that the anti-fibrotic effects of fluvoxamine are SERT-dependent, we performed
530 complementary gain- and loss-of-function experiments. The ability of fluvoxamine to
531 suppress TGF-β-induced fibrotic markers was abolished upon SERT knockdown (Fig.
532 8C). Furthermore, in mice with fibroblast-specific SERT overexpression (via AAV9),

fluvoxamine treatment significantly attenuated the associated increase in both ROS (by 32.5%) and Hic5 expression (by 28.6%) in cardiac fibroblasts (Fig. 8D). Collectively, these results demonstrate that SSRIs inhibit SERT activity, which attenuates the SERT-driven ROS-Hic5 signaling cascade, suppresses fibroblast activation, and provides a mechanistic basis for their anti-fibrotic effect in HFpEF.

Discussion

Despite its growing prevalence, heart failure with preserved ejection fraction (HFpEF) remains a syndrome in search of effective disease-modifying therapies. Pathological myocardial remodeling, characterized by hypertrophy and progressive interstitial fibrosis, is a central driver of diastolic dysfunction and clinical progression in HFpEF[42]. Identification of novel cellular pathways that govern this fibrotic process is therefore essential for therapeutic development. In this study, through cMAP screening, clinical data and mechanistic dissection, we identify the serotonin transporter (SERT) as a novel, druggable regulator of fibroblast activation in HFpEF and elucidate a complete SERT/MAO-A/ROS/Hic5 signaling axis in cardiac fibroblasts. We further demonstrate that selective serotonin reuptake inhibitors (SSRIs) confer direct anti-fibrotic and functional benefits by inhibiting this SERT-mediated pathway. Our findings bridge the clinical observation and molecular mechanism in HFpEF. Our clinical data first revealed an association between SSRI use and attenuated cardiac function and outcomes in two independent HFpEF cohorts. Moreover, in our two-hit mouse model of HFpEF, the SSRI fluvoxamine directly improved diastolic function and reduced

554 fibrosis. These data, combined with the elucidated SERT-Hic5 molecular pathway in
555 cardiac fibroblasts, provide experimental support for a cardioprotective mechanism [43,
556 44] that is at least partly independent of the drug's established psychiatric effects.

557 Cardiac fibroblasts constitute the most abundant cell type in the heart[45] and are the
558 primary effectors of extracellular matrix deposition[46]. In HFpEF, a complex interplay
559 of metabolic, inflammatory, and hemodynamic stimuli drives these cells toward a
560 pathological, activated myofibroblast phenotype[47]. Our study reveals that SERT, the
561 canonical target of SSRIs, is specifically upregulated within cardiac fibroblasts in
562 HFpEF. This cell-type-specific expression is functionally important: although SSRIs
563 suppressed hypertrophy markers in cardiomyocytes *in vitro*, our *in vivo* gain- and loss-
564 of-function experiments definitively established that fibroblast-specific manipulation
565 of SERT-Hic5 axis was both necessary and sufficient to drive or ameliorate diastolic
566 dysfunction and fibrosis. This finding repositions SERT from its traditional role in
567 neuronal serotonin reuptake[48] to a direct modulator of cardiac fibroblast activation in
568 HFpEF, revealing a pathophysiological function distinct from systemic serotonin
569 signaling.

570 To decipher how SERT activation promotes fibrosis, we delineated a downstream
571 axis converging on the transcription co-regulator Hic5 (TGFB1I1). Transcriptomic
572 analysis identified Hic5 as a key node downstream of SERT. Mechanistically, SERT-
573 mediated uptake of serotonin (5HT) into fibroblasts fuels its degradation by
574 mitochondrial monoamine oxidase A (MAO-A), a process that generates reactive

oxygen species (ROS). This SERT-driven oxidative stress potently upregulates Hic5, which in turn orchestrates the expression of a pro-fibrotic gene program, including collagens, fibronectin, and αSMA. Genetic ablation of Hic5 blocked the fibrogenic effects of SERT, confirming its indispensable role. Thus, we define a novel SERT/MAO-A/ROS/Hic5 pathway that directly links serotonin transport to fibroblast activation via oxidative stress-responsive transcription.

An important consideration is whether this pathway is unique to HFpEF. Our human myocardial biopsy data revealed higher SERT and Hic5 expression in HFpEF versus HFrEF samples, with SERT correlating with diastolic dysfunction severity and Hic5 correlating with left ventricular ejection fraction. This observation aligns with the distinct pathophysiological landscapes of the two syndromes: HFpEF is strongly characterized by a pro-fibrotic phenotype and systemic inflammation[49], which may support fibroblast-centric SERT upregulation. In contrast, HFrEF is dominated by cardiomyocyte loss[6] and systolic dysfunction[45]. This apparent paradox—more extensive fibrosis but lower SERT/Hic5 expression in HFrEF—likely reflects the fundamentally different modes of fibrosis in the two syndromes: replacement scarring in HFrEF versus diffuse interstitial fibrosis in HFpEF. This distinction may explain why SSRIs failed to show benefit in HFrEF patients in prior trials such as MOOD-HF, and it identifies HFpEF as the appropriate clinical context for evaluating SSRIs as anti-fibrotic therapy. Our current data showing robust effects in a validated HFpEF model and clinical HFpEF cohorts, strongly support the pathogenic relevance of the SERT-

596 Hic5 axis particularly in HFpEF, while a definitive comparison requires further studies
597 in different heart failure phenotypes.

598 The therapeutic implications of this pathway are underscored by SSRIs, yet our
599 work provides a fundamentally new perspective on their mechanism. Prior clinical
600 studies on SSRIs and cardiovascular outcomes have yielded mixed results, largely
601 focusing on depression comorbidity[50], platelet inhibition[43], or arrhythmia risk[51]. In
602 contrast, we demonstrate a direct, cardioprotective, and anti-fibrotic mechanism:
603 fluvoxamine treatment suppressed the entire SERT-ROS-Hic5 cascade—reducing
604 intracellular ROS, decreasing Hic5 expression, and inhibiting fibroblast activation—in
605 a manner strictly dependent on SERT inhibition. This SERT-Hic5 axis intersects with
606 yet distinctively extends known fibrotic pathways. While TGF-β is a master regulator
607 and can also induce Hic5, SERT provides a parallel and potent activation signal via
608 ROS, positioning Hic5 as a convergent hub for multiple pro-fibrotic stimuli.
609 Consequently, the observation that widely used, well-tolerated SSRIs can precisely
610 modulate this axis reframes their potential value in cardiology, moving beyond indirect
611 associations to targeted pathway inhibition. The repurposing of SSRIs could offer a
612 strategic approach to mitigate fibrosis in HFpEF, a condition desperately lacking such
613 targeted therapies.

614 Our study has limitations, including its retrospective nature of clinical components
615 and the inherent constraints of animal models. Despite covariate adjustment using
616 IPTW, residual confounding from unmeasured factors such as severity of depression,

objective measures of physical activity, levels of social support, and the detailed use of other psychotropic medications, cannot be excluded. The observed cardiac benefits may be indirectly provided by SSRIs through the reduction of depressive symptoms, such as increased energy and motivation promoting physical activity in turn, better autonomic nervous system balance, and better self-care in general. Additionally, despite the application of IPTW, our secondary validation utilizing the MIMIC-IV database remains susceptible to collider stratification bias: ICU admission is a conditioning event that can generate spurious statistical associations between SSRI use and clinical outcomes if both factors independently influence admission likelihood. Furthermore, the potential cardiovascular risks associated with SSRIs warrant consideration. Some SSRIs may prolong QT-interval as a risk factor for arrhythmias[52], and increase bleeding risk due to platelet aggregation[53], thereby, limiting their applicability in certain HFpEF populations. Thus, prospective evaluation of SSRIs in HFpEF must carefully balance potential benefits against these established risks. Moreover, the MIMIC-IV cohort comprises critically ill patients and does not represent the broader ambulatory HFpEF population that would be the target for chronic SSRI therapy. Therefore, these clinical observations should be interpreted as correlative rather than causal, and prospective randomized controlled trials are needed to evaluate the efficacy and safety of SSRIs specifically in HFpEF.

The preclinical dose of fluvoxamine (10 mg/kg/d) used in our mouse model is within the standard antidepressant range reported[54,55] and was not associated with overt

adverse effects in our experiments. In addition, our LC-MS/MS measurements confirmed that this dosing regimen achieves steady-state plasma concentrations near the lower end of the human therapeutic window, supporting the translational relevance of our preclinical findings. However, the use of SSRIs in HFpEF patients without depressive symptoms would require rigorous assessment of behavioral and psychological impacts. The “two-hit” mouse model effectively replicated several hallmarks of early HFpEF, including diastolic dysfunction and cardiac hypertrophy. However, this model cannot fully reflect the systemic complexity of human HFpEF, such as pulmonary hypertension, chronic kidney disease, and skeletal muscle abnormalities. Besides, this study used only male mice to avoid the potential confounding effects of estrogen fluctuations in females, consistent with established HFpEF modeling approaches[56]. However, this limits the generalizability of our findings to female patients, in whom HFpEF prevalence is higher. Sex differences in SERT expression, serotonin signaling, and SSRI pharmacokinetics have been described. Therefore, future studies should include female animals to validate the findings and determine whether sex-specific differences exist in the SERT-ROS-Hic5 axis.

Future work should prospectively validate SSRI efficacy and explore SERT’s role in other cell types. Nevertheless, converging evidence across disciplines establishes the fibroblast SERT-ROS-Hic5 axis as a novel contributor to HFpEF. Our findings not only advance the understanding of HFpEF pathophysiology but also nominate SSRIs as a ready-for-trial therapeutic strategy and delineate a new target space for antifibrotic drug

development.

Abbreviations

5HT – 5-Hydroxytryptamine (Serotonin)

HFpEF – Heart Failure with preserved Ejection Fraction

Hic5 – Hydrogen Peroxide Inducible Clone 5 (Gene Name: TGFB1I1)

L-NAME – N-ω--Nitro-L-arginine methyl ester

LNAC – N-Acetyl-L-cysteine

MAO-A – Monoamine Oxidase A

ROS – Reactive Oxygen Species

SERT – Serotonin Transporter

SLC6A4 – Solute Carrier Family 6 Member 4

SSRI – Selective Serotonin Reuptake Inhibitor

References

1. Dunlay SM, Roger VL, Redfield MM. Epidemiology of heart failure with preserved ejection fraction. Nat Rev Cardiol. 2017;14:591–602.

2. Hamo CE, DeJong C, Hartshorne-Evans N, et al. Heart failure with preserved ejection fraction. Nat Rev Dis Primers. 2024;10:55.

3. Hamed, O., Reitz, C. J., Kuzmanov, U., Gramolini, S., Hu, M., Halpern, J., Billia, F., & Gramolini, A. O. (2026). Cardiac proteomic and phosphoproteomic profiling defines clinically relevant molecular subgroups in human heart failure. Nature cardiovascular research, 2026;5(10):1016-1033.

4. Bishu K, Hamdani N, Mohammed SF, et al. Sildenafil and B-type natriuretic peptide acutely phosphorylate titin and improve diastolic distensibility in vivo. Circulation. 2011;124:2882–2891.

5. Westermann D, Lindner D, Kasner M, et al. Cardiac inflammation contributes to changes in the extracellular matrix in patients with heart failure and normal ejection fraction. Circ Heart Fail. 2011;4:44–52.

6. Koehler, X. Severe obesity alters contractile function in heart failure with preserved ejection fraction. Nature cardiovascular research.2026;5: 667.

7. Schiattarella GG, Altamirano F, Kim SY, et al. Xbp1s-FoxO1 axis governs lipid accumulation and contractile performance in heart failure with preserved ejection fraction. Nat Commun. 2021;12:1684.

8. Hundertmark MJ, Birkhoelzer SM, Portwood C, et al. IMPROVE-DiCE, a 2-Part, Open-Label, Phase 2a Trial Evaluating the Safety and Effectiveness of Ninerafaxstat in Patients With Cardiometabolic Syndromes. Circulation. 2026;153(8):550-563.

9. Hahn VS, Petucci C, Kim MS, et al. Myocardial Metabolomics of Human Heart Failure With Preserved Ejection Fraction. Circulation. 2023;147:1147–1161.

10. Zhang K, Gan J, Wang B, et al. FGF21 protects against HFpEF by improving cardiac mitochondrial bioenergetics in mice. Nat Commun. 2025;16(1):1661.
11. Pepin ME, Konrad PJM, Nazir S, et al. Mitochondrial NNT Promotes Diastolic Dysfunction in Cardiometabolic HFpEF. Circ Res. 2025;136:1564–1578.
12. Stadiotti I, Santoro R, Scopece A, et al. Pressure Overload Activates DNA-Damage Response in Cardiac Stromal Cells: A Novel Mechanism Behind Heart Failure with Preserved Ejection Fraction? Front Cardiovasc Med. 2022;9:878268.
13. Paulus WJ, Zile MR. From Systemic Inflammation to Myocardial Fibrosis: The Heart Failure With Preserved Ejection Fraction Paradigm Revisited. Circ Res. 2021;128:1451–1467.
14. Campbell P, Rutten FH, Lee MM, Hawkins NM, Petrie MC. Heart failure with preserved ejection fraction: everything the clinician needs to know. Lancet. 2024;403:1083–1092.
15. Solomon SD, Vaduganathan M, L Claggett B, et al. Sacubitril/Valsartan Across the Spectrum of Ejection Fraction in Heart Failure. Circulation. 2020;141:352–361.
16. Marathonitis, A., Anastasiou, A., Vythoulkas-Biotis, N. et al. Myocardial extracellular volume reduction is associated with improved cardiac function after SGLT2 inhibitor therapy in HFpEF. Scientific Reports. 2026;ISSN 2045-2322.
17. Cunningham JW, Claggett BL, O'Meara E, et al. Effect of Sacubitril/Valsartan on Biomarkers of Extracellular Matrix Regulation in Patients With HFpEF. J Am Coll Cardiol. 2020;76:503–514.
18. Zhang W, Liu J, Fu Y, et al. Sacubitril/Valsartan Reduces Fibrosis and Alleviates

High-Salt Diet-Induced HFpEF in Rats. Front Pharmacol. 2021;12:600953.

19. Liu J, Zheng X, Zhang C, Zhang C, Bu P. Lcz696 Alleviates Myocardial Fibrosis After Myocardial Infarction Through the sFRP-1/Wnt/β-Catenin Signaling Pathway. Front Pharmacol. 2021;12:724147.

20. Stanko P, Repova K, Baka T, et al. Sacubitril/Valsartan Alleviates Cardiac Remodeling and Dysfunction in L-NAME-Induced Hypertension and Hypertensive Heart Disease. Biomedicines. 2024;12:733.

21. Deng Y, Xie M, Li Q, et al. Targeting Mitochondria-Inflammation Circuit by β-Hydroxybutyrate Mitigates HFpEF. Circ Res. 2021;128:232–245.

22. Butler J, Shah SJ, Petrie MC, et al. STEP-HFpEF Trial Committees and Investigators. Semaglutide versus placebo in people with obesity-related heart failure with preserved ejection fraction: a pooled analysis of the STEP-HFpEF and STEP-HFpEF DM randomised trials. Lancet. 2024;403:1635–1648.

23. Coleman JA, Green EM, Gouaux E. X-ray structures and mechanism of the human serotonin transporter. Nature. 2016;532:334–339.

24. Galli A, Petersen CI, deBlaquiere M, Blakely RD, DeFelice LJ. Drosophila serotonin transporters have voltage-dependent uptake coupled to a serotonin-gated ion channel. J Neurosci. 1997;17:3401–3411.

25. Bianchi P, Pimentel DR, Murphy MP, Colucci WS, Parini A. A new hypertrophic mechanism of serotonin in cardiac myocytes: receptor-independent ROS generation. FASEB J. 2005;19:641–643.

26. Shibanuma M, Mashimo J, Kuroki T, Nose K. Characterization of the TGF beta 1-

742 inducible hic-5 gene that encodes a putative novel zinc finger protein and its possible
743 involvement in cellular senescence. J Biol Chem. 1994;269:26767–26774.
744 27. Dabiri G, Tumbarello DA, Turner CE, Van de Water L. Hic-5 promotes the
745 hypertrophic scar myofibroblast phenotype by regulating the TGF-beta1 autocrine
746 loop. J Invest Dermatol. 2008;128:2518–2525.
747 28. Carneiro AM, Blakely RD. Serotonin-, protein kinase C-, and Hic-5-associated
748 redistribution of the platelet serotonin transporter. J Biol Chem. 2006;281:24769–
749 24780.
750 29. Carneiro AM, Ingram SL, Beaulieu JM, et al. The multiple LIM domain-containing
751 adaptor protein Hic-5 synaptically colocalizes and interacts with the dopamine
752 transporter. J Neurosci. 2002;22:7045–7054.
753 30. Shibanuma M, Kim-Kaneyama JR, Sato S, Nose K. A LIM protein, Hic-5, functions
754 as a potential coactivator for Sp1. J Cell Biochem. 2004;91:633–645.
755 31. Kim-Kaneyama JR, Shibanuma M, Nose K. Transcriptional activation of the c-fos
756 gene by a LIM protein, Hic-5. Biochem Biophys Res Commun. 2002;299:360–365.
757 32. Xu W, Goreczny GJ, Forsythe I, et al. Hic-5 regulates extracellular matrix-associated
758 gene expression and cytokine secretion in cancer associated fibroblasts. Exp Cell Res.
759 2024;435:113930.
760 33. Lin CH, Yu MC, Tung WH, et al. Connective tissue growth factor induces collagen I
761 expression in human lung fibroblasts through the Rac1/MLK3/JNK/AP-1 pathway.
762 Biochim Biophys Acta. 2013;1833:2823–2833.
763 34. Papismadov N, Levi N, Roitman L, et al. p21 regulates expression of ECM

components and promotes pulmonary fibrosis via CDK4 and Rb. EMBO J. 2024;43:5360–5380.

35. Schiattarella GG, Altamirano F, Tong D, et al. Nitrosative stress drives heart failure with preserved ejection fraction. Nature. 2019;568:351–356.

36. Gan L, Li R, Wang Q, et al. PAD2 disturbs cardiomyocyte calcium homeostasis by citrullinating SERCA2a protein in hemorrhagic shock induced arrhythmia. J Trauma Acute Care Surg. 2025;99:219–232.

37. Shah SJ, Kitzman DW, Borlaug BA, et al. Phenotype-Specific Treatment of Heart Failure With Preserved Ejection Fraction: A Multiorgan Roadmap. Circulation. 2016;134:73–90.

38. Ferreira FL, Bota DP, Bross A, Mélot C, Vincent JL. Serial evaluation of the SOFA score to predict outcome in critically ill patients. JAMA. 2001;286:1754–1758.

39. Miyamoto J, Tsuji M, Takeda H, et al. Characterization of the anxiolytic-like effects of fluvoxamine, milnacipran and risperidone in mice using the conditioned fear stress paradigm. Eur J Pharmacol. 2004;504:97–103.

40. Xie X, Wu X, Zhao D, et al. Fluvoxamine alleviates bleomycin-induced lung fibrosis via regulating the cGAS-STING pathway. Pharmacol Res. 2023;187:106577.

41. Weng L, Ye J, Yang F, et al. TGF-β1/SMAD3 Regulates Programmed Cell Death 5 That Suppresses Cardiac Fibrosis Post-Myocardial Infarction by Inhibiting HDAC3. Circ Res. 2023;133:237–251.

42. Peikert A, Fontana M, Solomon SD, Thum T. Left ventricular hypertrophy and myocardial fibrosis in heart failure with preserved ejection fraction: mechanisms and

786 treatment. Eur Heart J. 2026;47:37–53.
787 43. Serebruany VL, Glassman AH, Malinin AI, et al. Selective serotonin reuptake
788 inhibitors yield additional antiplatelet protection in patients with congestive heart
789 failure treated with antecedent aspirin. Eur J Heart Fail. 2003;5:517–521.
790 44. Angermann CE, Gelbrich G, Störk S, et al. MOOD-HF Investigators. Rationale and
791 design of a randomised, controlled, multicenter trial investigating the effects of
792 selective serotonin re-uptake inhibition on morbidity, mortality and mood in
793 depressed heart failure patients (MOOD-HF). Eur J Heart Fail. 2007;9:1212–1222.
794 45. Bergmann O, Zdunek S, Felker A, et al. Dynamics of Cell Generation and Turnover
795 in the Human Heart. Cell. 2015;161:1566–1575.
796 46. Willmer M, Szardien S, Kraft D, et al. Extracellular matrix remodeling in early
797 cardiac fibrosis and diastolic dysfunction. Eur Heart J. 2013;34:P4197.
798 47. Van Linthout S, Matz I, González A, Davis J. Cardiac fibroblasts in myocardial injury
799 and heart failure. Eur Heart J. 2025;ehaf902.
800 48. Soiza-Reilly M, Meye FJ, Olusakin J, et al. SSRIs target prefrontal to raphe circuits
801 during development modulating synaptic connectivity and emotional behavior. Mol
802 Psychiatry. 2019;24:726–745.
803 49. Sakamoto D, Seo M, Yamada T, et al. Prognostic impact of the serial change of a
804 systemic inflammation-nutrition index in patients with heart failure with preserved
805 ejection fraction: insights from pursuit-hfpef registry. Eur Heart J.
806 2022;43:ehac544.876.
807 50. Hare DL, Toukhsati SR, Johansson P, Jaarsma T. Depression and cardiovascular

disease: a clinical review. Eur Heart J. 2014;35:1365–1372.

51. Fanoe S, Kristensen D, Fink-Jensen A, et al. Risk of arrhythmia induced by psychotropic medications: a proposal for clinical management. Eur Heart J. 2014;35:1306–1315.

52. Beach, S. R., Kostis, W. J., Celano, C. M., et al. Meta-analysis of selective serotonin reuptake inhibitor-associated QTc prolongation. The Journal of clinical psychiatry. 2014, 75(5): e441-e449.

53. Picado-Loaiza S, Valverde NNG, Sánchez FZ, et al. Selective Serotonin Reuptake Inhibitors Increase Gastrointestinal but Not Other Site Bleeding Risk in Left Ventricular Assist Device Patients: A Systematic Review and Meta-Analysis. J Cardiothorac Vasc Anesth. 2025, 39(12): 3525-3533.

54. Xu D, Wang C, Zhu X, et al. The antidepressant-like effects of fluvoxamine in mice involve the mTOR signaling in the hippocampus and prefrontal cortex. Psychiatry Res. 2020;285:112708.

55. Teng S, Yang Y, Zhang W, et al. Antidepressant fluoxetine alleviates colitis by reshaping intestinal microenvironment. Cell Commun Signal. 2024;22(1):176.

56. Kass, D.A. Modeling HFpEF in animals. Nat Cardiovasc Res. 2025;4, 1589–1591.

Authors' contributions

Ming Zheng and Jingjing Ye designed the project. Mingyang Zhao, Geng Bai and Xin

Wang performed cell experiments and animal experiments. Geng Bai, Jingjing Ye, Songtao Jiang and Tao Shen collected and analyzed the clinical data and provided human myocardial biopsy samples. Ming Zheng, Jingjing Ye and Mingyang Zhao wrote the original manuscript. All authors contributed to data interpretation, experimental design, data analysis, and approved the final version for submission.

Competing interests

The authors declare that they have no competing interests.

Availability of data and materials

The data underlying this article will be shared on reasonable request to the corresponding author.

Consent for publication

All authors give their consents to publish this work.

Figures and figure legends

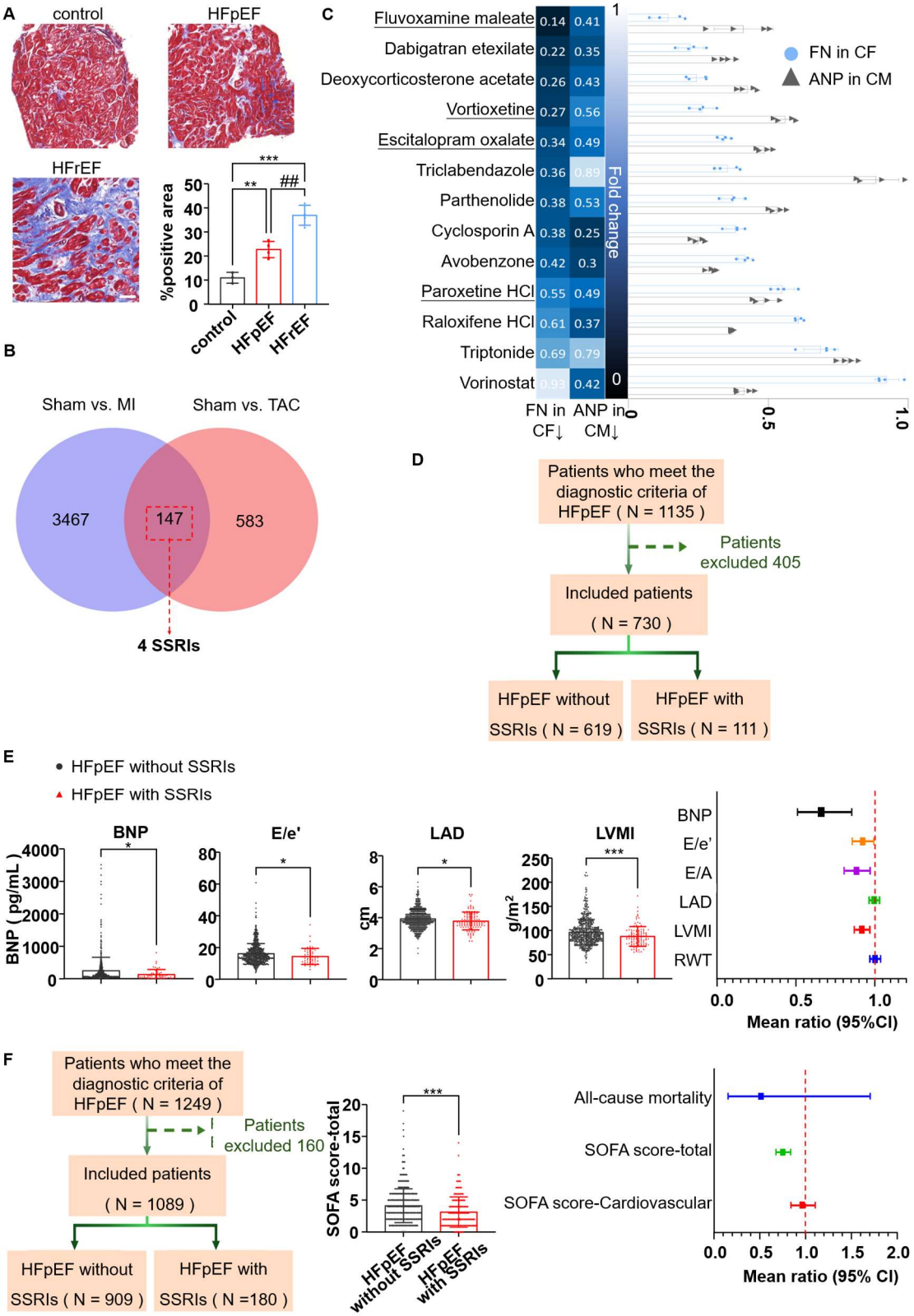
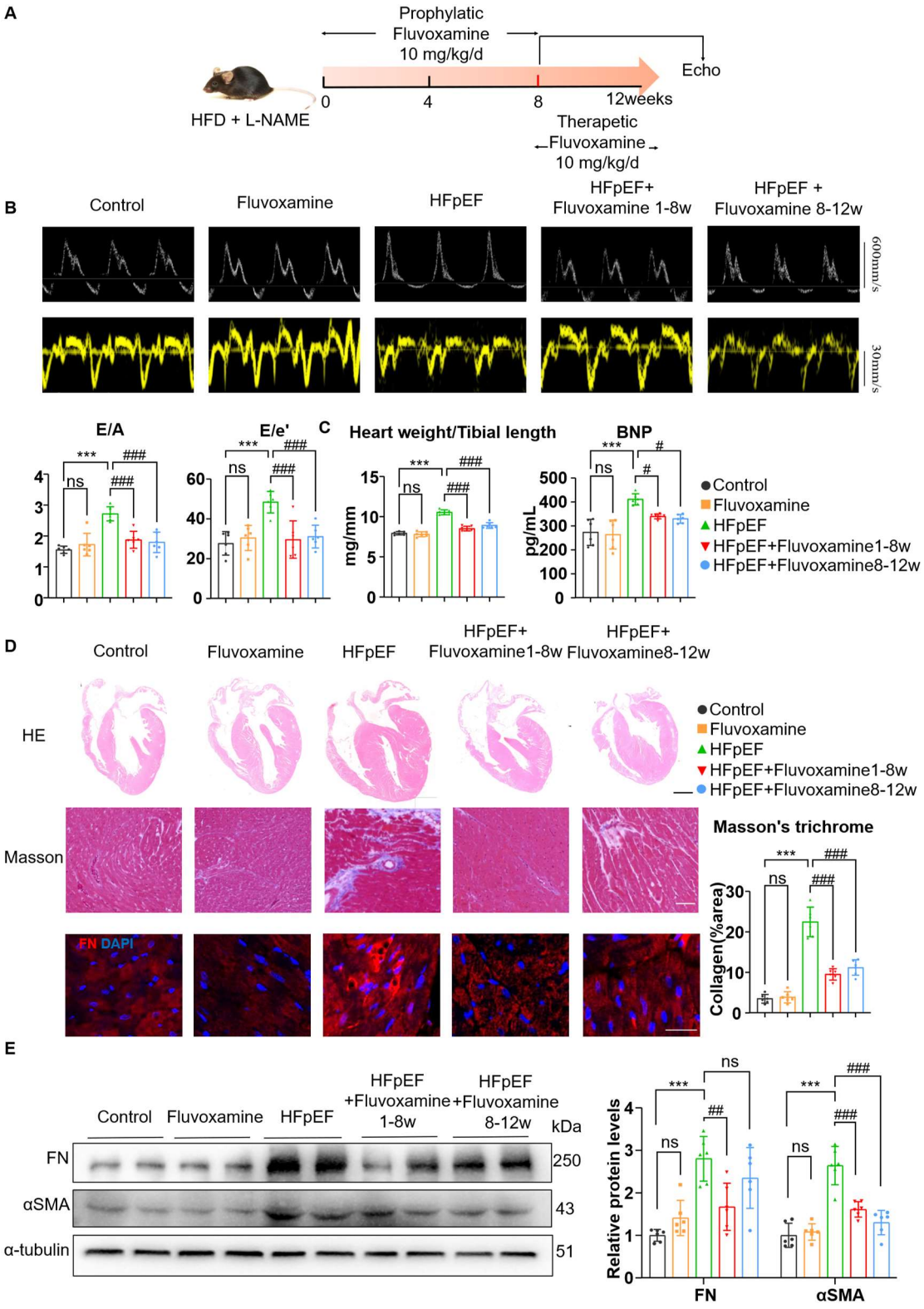


Figure 1. SSRI use is associated with improved diastolic function and reduced

Sequential Organ Failure Assessment (SOFA) Score in HFpEF patients and inhibits remodeling in vitro. A, Masson Staining and percentage area of Masson's trichrome staining of myocardial tissue from patients. n = 3-4, statistical significance was assessed by Kruskal Wallis H followed by Bonferroni's post hoc test. Scale bar = 50 μm. **B**, Drug screening using the cMAP database based on cardiac transcriptome data from mice 28 days after myocardial infarction modeling and from mice with transverse aortic constriction (TAC)-induced hypertrophic cardiomyopathy. **C**, Heatmap showing the effects of 13 on the expression of the hypertrophic marker atrial natriuretic peptide (ANP) in cardiomyocytes and the fibrotic marker fibronectin (FN) in fibroblasts. Four SSRIs (fluvoxamine maleate, vortioxetine, escitalopram oxalate, and paroxetine HCl) that overlapped with cMAP predictions consistently suppressed ANP and FN upregulation. **D**, Flowchart of HFpEF patient inclusion and exclusion criteria. **E,** Left, statistical analysis of characteristics in HFpEF patients with and without SSRI use, statistical significance was assessed by unpaired 2-tailed Student t test. , Right, forest plot showing the ratio of means (with 95% CI) for each parameter comparing SSRI users to non-users, derived from multivariable gamma generalized linear models. **F**, Left, flowchart of patient inclusion and exclusion criteria in MIMIC database. Middle, SOFA score on admission in HFpEF patients with and without SSRI use, statistical significance was assessed by unpaired 2-tailed Student t test. Right, forest plot showing the ratio of means (with 95% CI) for each parameter comparing SSRI users to non-users, derived from multivariable gamma generalized linear models.

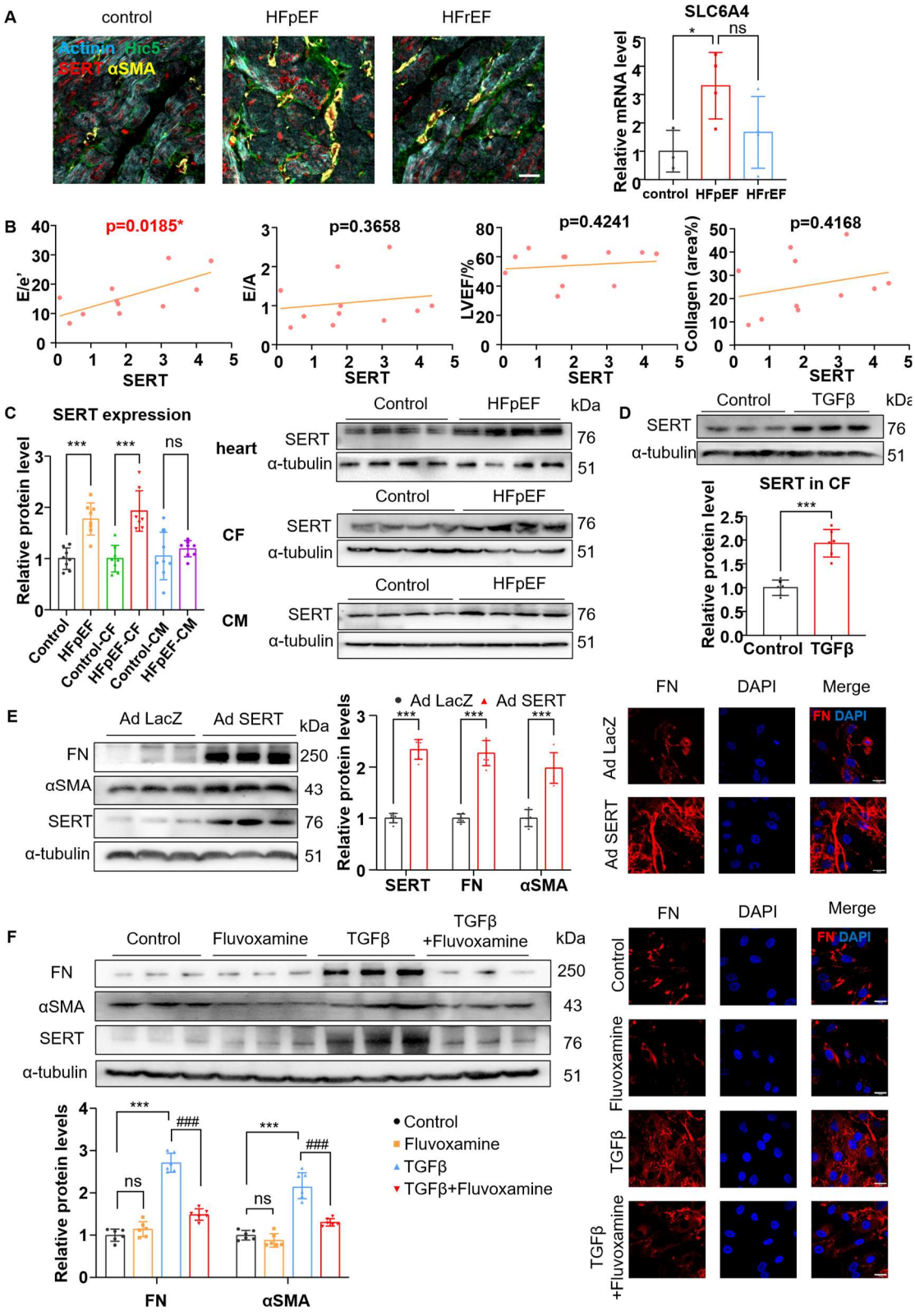


866

867 **Figure 2, SSRIs improve diastolic function and ameliorate cardiac hypertrophy**

868 **and fibrosis in HFpEF mouse model. A,** Schematic diagram of preventive or

therapeutic SSRI administration in HFpEF mice. **B**, Representative transmitral flow and tissue Doppler echocardiography images, E/A ratio, and E/e' ratio. n = 6 mice per group. Statistical significance was assessed by One way ANOVA analysis followed by Bonferroni's post hoc test. **C**, Serum BNP levels and heart weight-to-tibia length ratio in HFpEF mice treated with Fluvoxamine or PBS. n = 6 mice per group. Statistical significance was assessed by One way ANOVA analysis followed by Bonferroni's post hoc test. **D**, HE, Masson and FN immunofluorescence Staining of Myocardial Tissue from mice. Scale bar = 500μm (HE), 100μm (Masson) or 25μm (FN), along with the percentage area of Masson's trichrome staining. n = 6 mice per group. Statistical significance was assessed by One way ANOVA analysis followed by Bonferroni's post hoc test. **E**, Representative Western blot and average data showing protein levels of fibronectin (FN) and alpha smooth muscle actin (αSMA) in heart tissues. n = 6 mice per group. Statistical significance was assessed by One way ANOVA analysis followed by Bonferroni's post hoc test.



883

884 **Figure 3. SERT promotes fibroblast activation. A**, Representative

885 immunofluorescence staining images showing SERT in myocardial tissue from patients,

and quantitative real-time PCR analysis of *SLC6A4* mRNA levels in myocardial tissue from patients (n = 3-4, statistical significance was assessed by Kruskal Wallis H followed by Bonferroni's post hoc test) Scale bar = 20 μm. **B**, Correlation analyses between *SLC6A4* mRNA exprssion and E/e' ratio, E/A ratio, left ventricular ejection fraction (LVEF). and the percentage area of Masson's trichrome staining, n = 11. **C**, Representative Western blot and average data showing protein levels of SERT in heart tissues, cardiomyocytes, and cardiac fibroblasts. n = 8 independent experiments. Statistical significance was assessed by One way ANOVA analysis followed by Bonferroni's post hoc test. **D**, Representative Western blot and average data showing protein levels of SERT in cardiac fibroblasts treated with or without 10 ng/mL TGF-β1 (transforming growth factor-β1). n = 6 independent experiments. Statistical significance was assessed by unpaired 2-tailed Student *t* test. **E**, Representative Western blot and average data showing protein levels of SERT, fibronectin (FN) and alpha smooth muscle actin (αSMA) in cardiac fibroblasts transfected with Ad-SERT or Ad-LacZ. n = 6 independent experiments. Statistical significance was assessed by unpaired 2-tailed Student *t* test. Immunofluorescence staining showing FN in corresponding groups. Scale bar = 20 μm. **F**, Representative Western blot and average data showing protein levels of fibronectin (FN) and alpha smooth muscle actin (αSMA) in cardiac fibroblasts treated with or without 10 ng/mL TGF-β1 and 10μM Fluvoxamine. n = 6 independent experiments. Statistical significance was assessed by unpaired 2-tailed Student *t* test. Immunofluorescence staining showing FN in cardiac fibroblasts under the same condition. Scale bar = 20 μm.

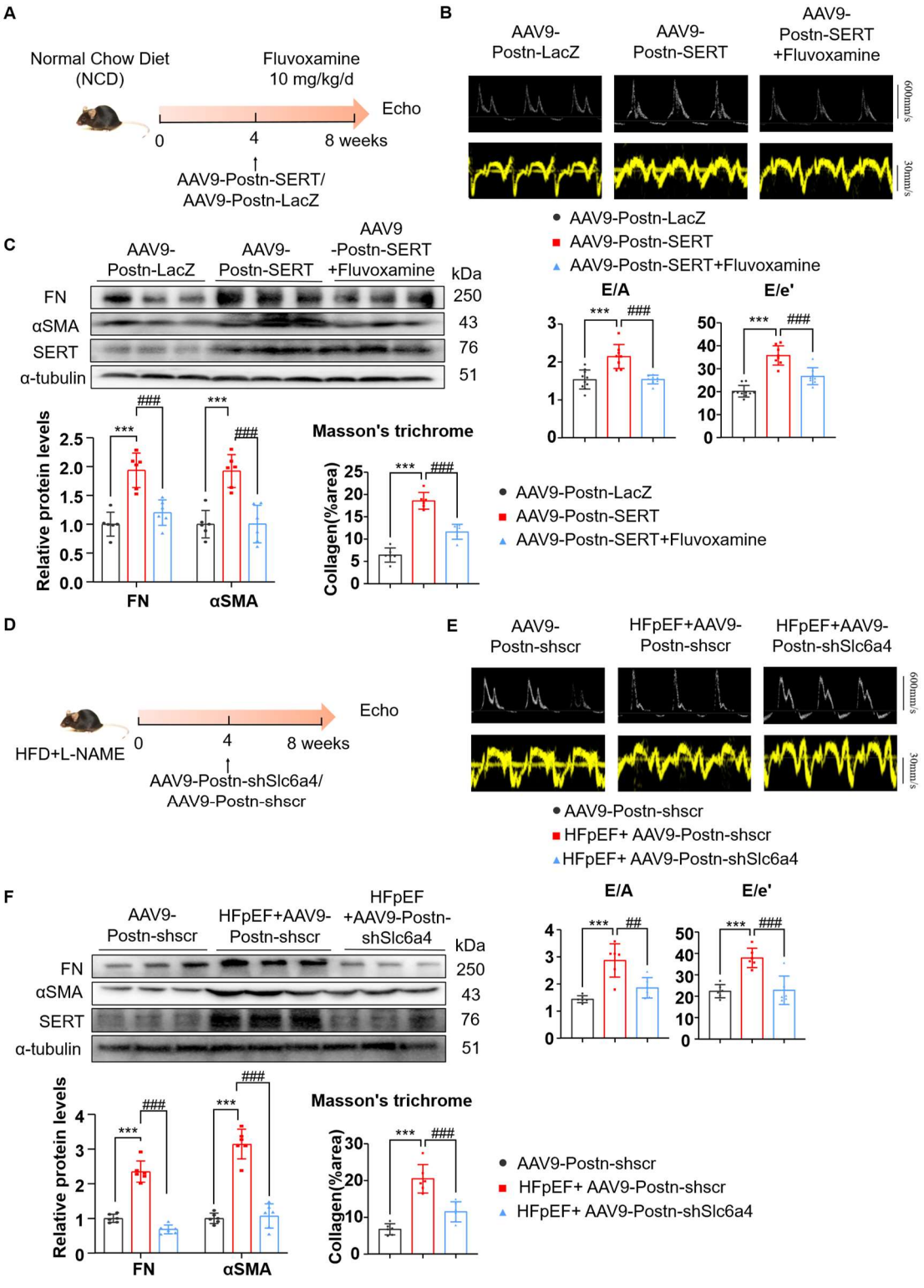


Figure 4. SERT promotes cardiac fibrosis. A, Schematic diagram of fibroblast-specific SERT overexpression in wild-type C57BL/6J mouse hearts using AAV9 driven

by the Postn promoter (AAV9-Postn-SERT) or AAV9-Postn-LacZ as control groups. Fluvoxamine is administered intraperitoneally 10 mg/kg/d. **B**, Representative transmitral flow and tissue Doppler echocardiography images, E/A ratio, and E/e' ratio. n = 8-10 mice per group. Statistical significance was assessed by One way ANOVA analysis followed by Bonferroni's post hoc test. **C**, Representative Western blot and average data showing protein levels of FN and αSMA in heart tissues, along with the percentage area of Masson's trichrome staining. n = 6 mice per group. Statistical significance was assessed by One way ANOVA analysis followed by Bonferroni's post hoc test. **D**, Schematic diagram of cardiac fibroblast-specific SERT knockdown in mice subjected to the HFpEF induction protocol, using AAV9 driven by the Postn promoter (AAV9-Postn-shSlc6a4) or AAV9-Postn- scramble shRNA as control groups. **E**, Representative transmitral flow and tissue Doppler echocardiography images, E/A ratio, and E/e' ratio. n = 6 mice per group. Statistical significance was assessed by One way ANOVA analysis followed by Bonferroni's post hoc test. **F**, Representative Western blot and average data showing protein levels of FN and αSMA in heart tissues, along with the percentage area of Masson's trichrome staining. n = 6 mice per group. Statistical significance was assessed by One way ANOVA analysis followed by Bonferroni's post hoc test.

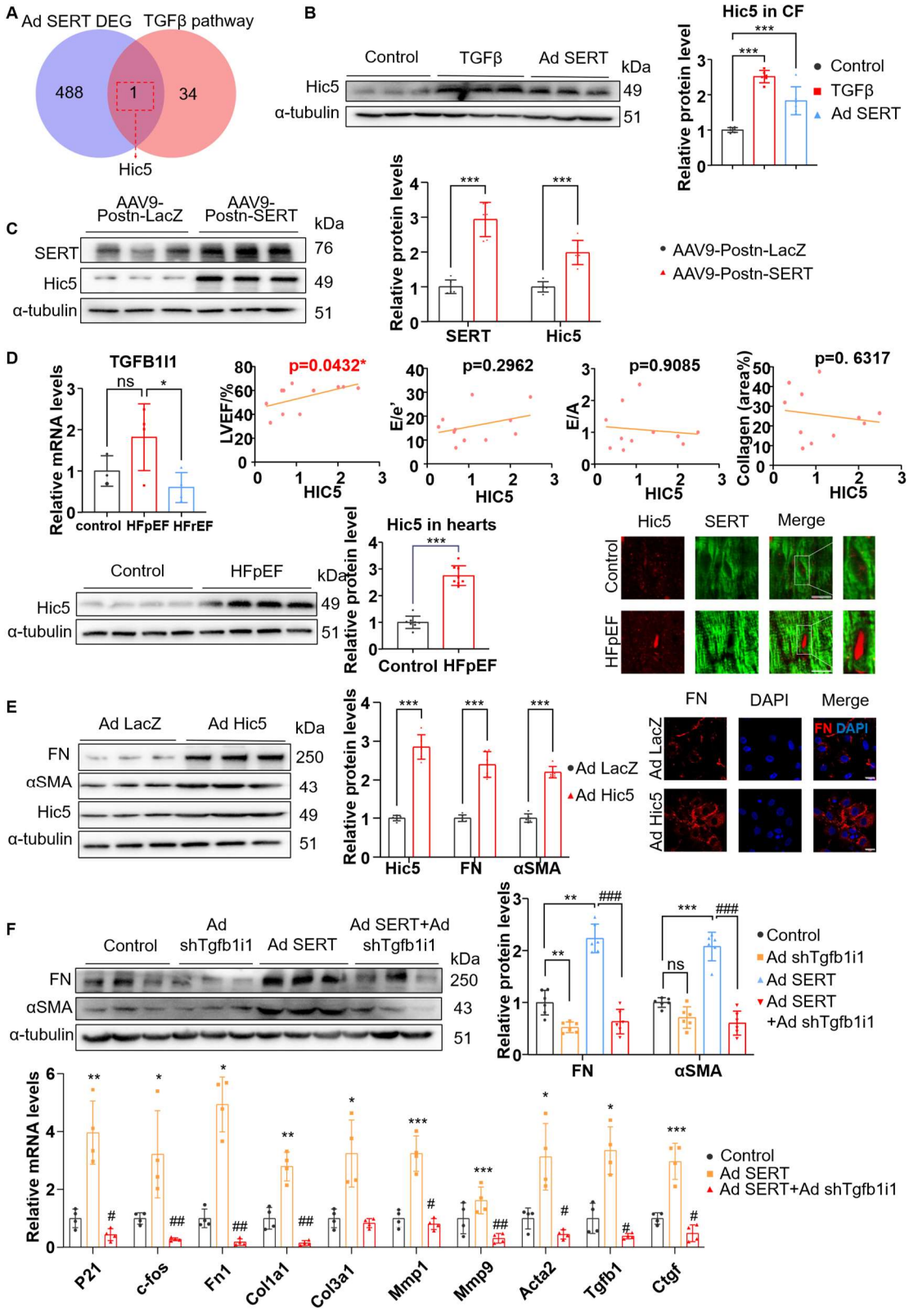
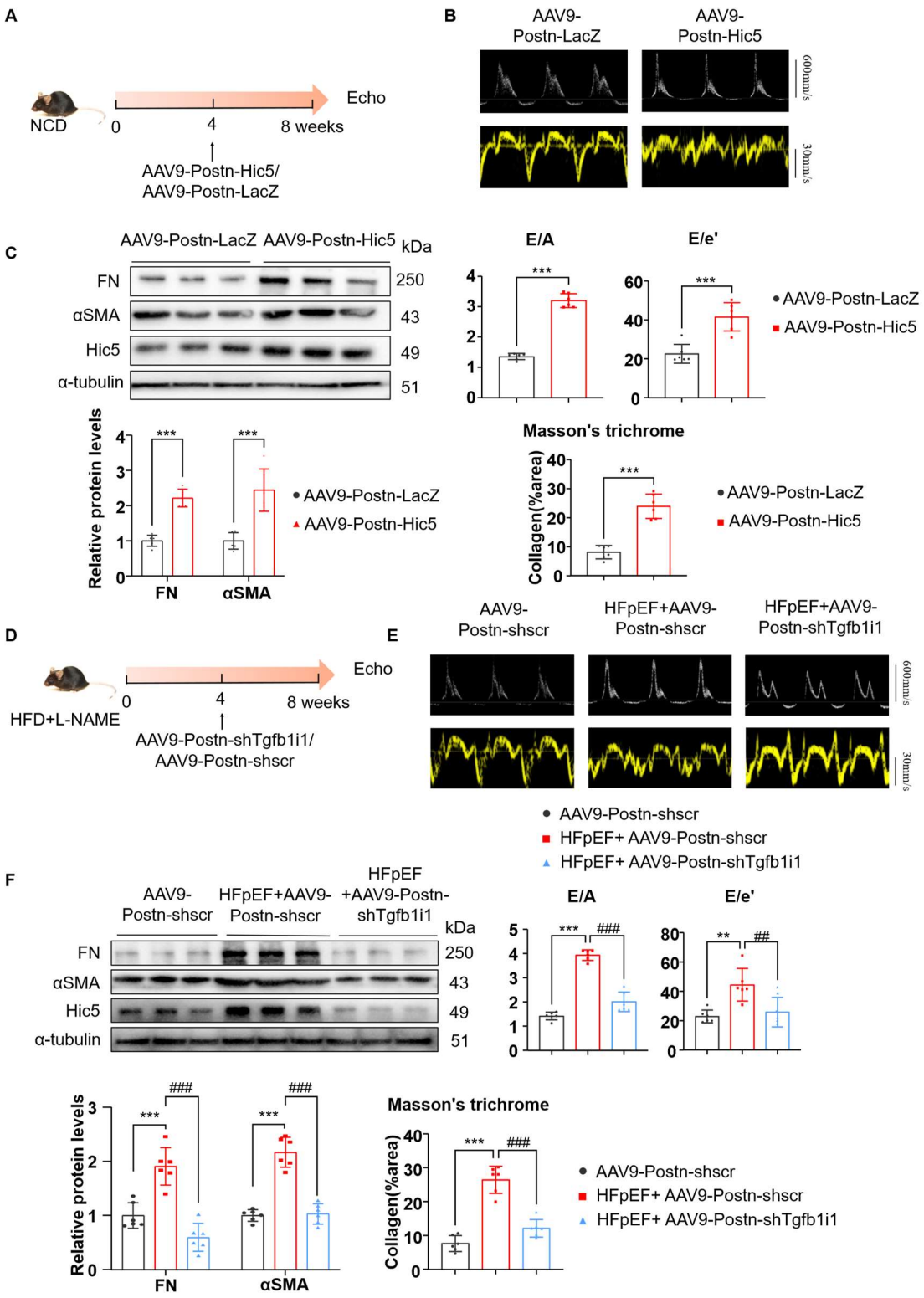


Figure 5. SERT promotes fibroblast activation via Hic5. A, Transcriptomic analysis of SERT-overexpressing fibroblasts, intersected with factors associated with TGFβ-

induced fibrosis. **B**, Representative Western blot and average data showing Hic5 protein levels in cardiac fibroblasts treated with or without 10 ng/mL TGF-β1 (transforming growth factor-β1) or transfected with Ad-SERT. n = 6 independent experiments. Statistical significance was assessed by One way ANOVA analysis followed by Bonferroni's post hoc test. **C**, Representative Western blot and average data showing protein levels of SERT and Hic5 in isolated cardiac fibroblasts from mice injecting AAV9 driven by the Postn promoter (AAV9-Postn-SERT) or AAV9-Postn-LacZ as control groups. n = 6 independent experiments. Statistical significance was assessed by unpaired 2-tailed Student *t* test. **D**, **Up**, Quantitative real-time PCR analysis of *TGFB1I1* mRNA levels in myocardial tissue from patients (n = 3-4 , statistical significance was assessed by Kruskal Wallis H followed by Bonferroni's post hoc test), along with correlation analyses between *TGFB1I1* mRNA exprssion and E/e' ratio , E/A ratio, left ventricular ejection fraction (LVEF) , and the percentage area of Masson's trichrome staining, n = 11; **Down**, representative Western blot and average data showing Hic5 protein levels in heart tissues, along with immunofluorescence staining of Hic5 and SERT in heart tissues from wild-type control (Control) and HFpEF mice. Scale bar = 10 μm. n = 8 mice per group. Statistical significance was assessed by unpaired 2-tailed Student *t* test. **E**, Representative Western blot and average data showing protein levels of Hic5, FN and αSMA in cardiac fibroblasts transfected with Ad-Hic5 or Ad-LacZ; n = 6 independent experiments. Statistical significance was assessed by unpaired 2-tailed Student *t* test. Immunofluorescence staining showing FN in corresponding groups. Scale bar = 20 μm. **F**, **Up**, Representative Western blot and average data showing

protein levels of FN and αSMA in cardiac fibroblasts transfected with or without Ad-SERT and Ad-shTgfb1i1. n = 6 independent experiments. Statistical significance was assessed by One way ANOVA analysis followed by Bonferroni's post hoc test. **Down,** quantitative real-time PCR analysis of P21, c-fos, Fn1, Col1a1, Col3a1, Mmp1, Mmp9, Acta2, Tgfb1 and Ctgf mRNA levels in rat neonatal cardiac fibroblasts transfected with or without Ad-SERT and Ad-shTgfb1i1. n = 4 independent experiments. Statistical significance was assessed by Kruskal Wallis H followed by Bonferroni's post hoc test.

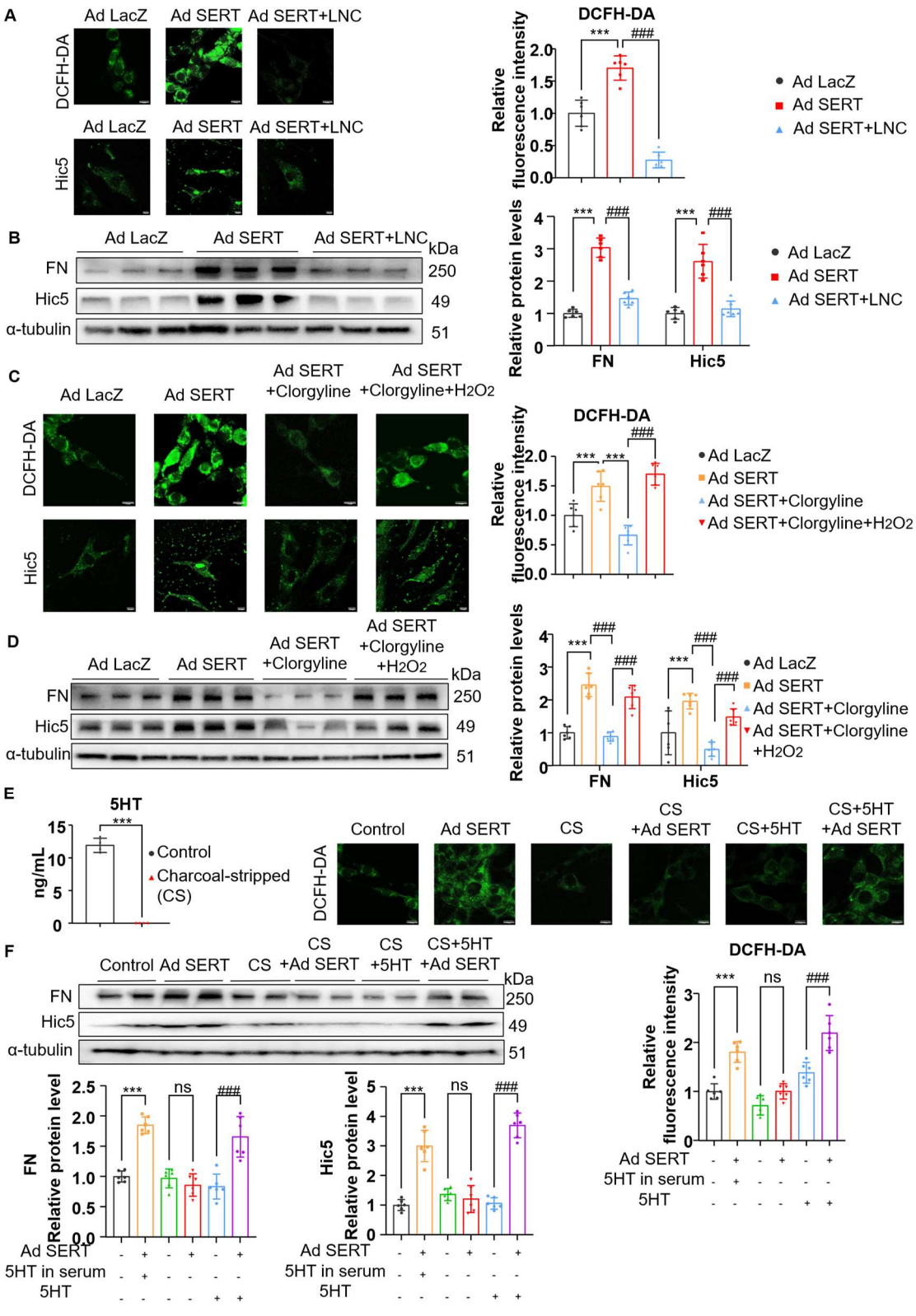


961

962 **Figure 6. Hic5 promotes fibroblast activation and cardiac fibrosis. A**, Schematic

963 diagram of fibroblast-specific Hic5 overexpression in wild-type C57BL/6J mouse

hearts using AAV9 driven by the Postn promoter (AAV9-Postn-Hic5) or AAV9-Postn-LacZ as control groups. **B**, Representative transmitral flow and tissue Doppler echocardiography images, E/A ratio, and E/e' ratio. n = 6 mice per group. Statistical significance was assessed by One way ANOVA analysis followed by Bonferroni's post hoc test. **C**, Representative Western blot and average analysis of FN and αSMA protein levels in heart tissues, along with the percentage area of Masson's trichrome staining. n = 6 mice per group. Statistical significance was assessed by One way ANOVA analysis followed by Bonferroni's post hoc test. **D**, Schematic diagram of cardiac fibroblast-specific Hic5 knockdown in mice subjected to the HFpEF induction protocol, using AAV9 driven by the Postn promoter (AAV9-Postn-shTgfb1i1) or AAV9-Postn-scramble shRNA as control groups. **E**, Representative transmitral flow and tissue Doppler echocardiography images, E/A ratio, and E/e' ratio. n = 6 mice per group. Statistical significance was assessed by One way ANOVA analysis followed by Bonferroni's post hoc test. **F**, Representative Western blot and average data showing protein levels of FN and αSMA in heart tissues, along with the percentage area of Masson's trichrome staining. n = 6 mice per group. Statistical significance was assessed by One way ANOVA analysis followed by Bonferroni's post hoc test.



981

982 **Figure 7. SERT enhances 5HT uptake, and MAO-A-mediated degradation of 5HT**

983 **generates ROS to promote Hic5 expression. A**, SERT overexpression promotes ROS

production and Hic5 expression in cardiac fibroblasts. Intracellular ROS levels were measured using the fluorescent probe DCFH-DA. n = 6 independent experiments. Statistical significance was assessed by One way ANOVA analysis followed by Bonferroni's post hoc test. Immunofluorescence staining showing Hic5 expression. Scale bar = 10 μm. **B**, Representative Western blot and average analysis of FN and Hic5 protein levels in cardiac fibroblasts transfected with Ad-SERT or Ad-LacZ and treated with or without 100μM N-acetyl-L-cysteine (LNC). n = 6 independent experiments. Statistical significance was assessed by One way ANOVA analysis followed by Bonferroni's post hoc test. **C**, SERT overexpression promotes ROS production and Hic5 transcription, which is inhibited by the MAO-A inhibitor clorgyline. Intracellular ROS levels were measured using DCFH-DA. n = 6 independent experiments. Statistical significance was assessed by One way ANOVA analysis followed by Bonferroni's post hoc test. Hic5 expression was detected by immunofluorescence staining. Scale bar = 10 μm. **D**, Representative Western blot and average analysis of FN and Hic5 protein levels in cardiac fibroblasts transfected with Ad-SERT or Ad-LacZ and treated with or without 10μM clorgyline. n = 6 independent experiments. Statistical significance was assessed by One way ANOVA analysis followed by Bonferroni's post hoc test. **E**, **Left**, Mass spectrometry measuring Fetal Bovine Serum 5HT levels. n = 4 independent experiments. Statistical significance was assessed by Kruskal Wallis H followed by Bonferroni's post hoc test. **Right**, SERT overexpression increases ROS in a manner dependent on the presence of 5HT in the culture medium. Cardiac fibroblasts were transfected with Ad-SERT or Ad-LacZ and cultured in normal serum or charcoal-

stripped serum. Scale bar = 10 μm. n = 6 independent experiments. Statistical significance was assessed by One way ANOVA analysis followed by Bonferroni's post hoc test. **F**, Representative Western blot and average analysis of FN and Hic5 protein levels in cardiac fibroblasts transfected with Ad-SERT or Ad-LacZ and cultured in normal serum or charcoal-stripped serum. n = 6 independent experiments. Statistical significance was assessed by One way ANOVA analysis followed by Bonferroni's post hoc test.

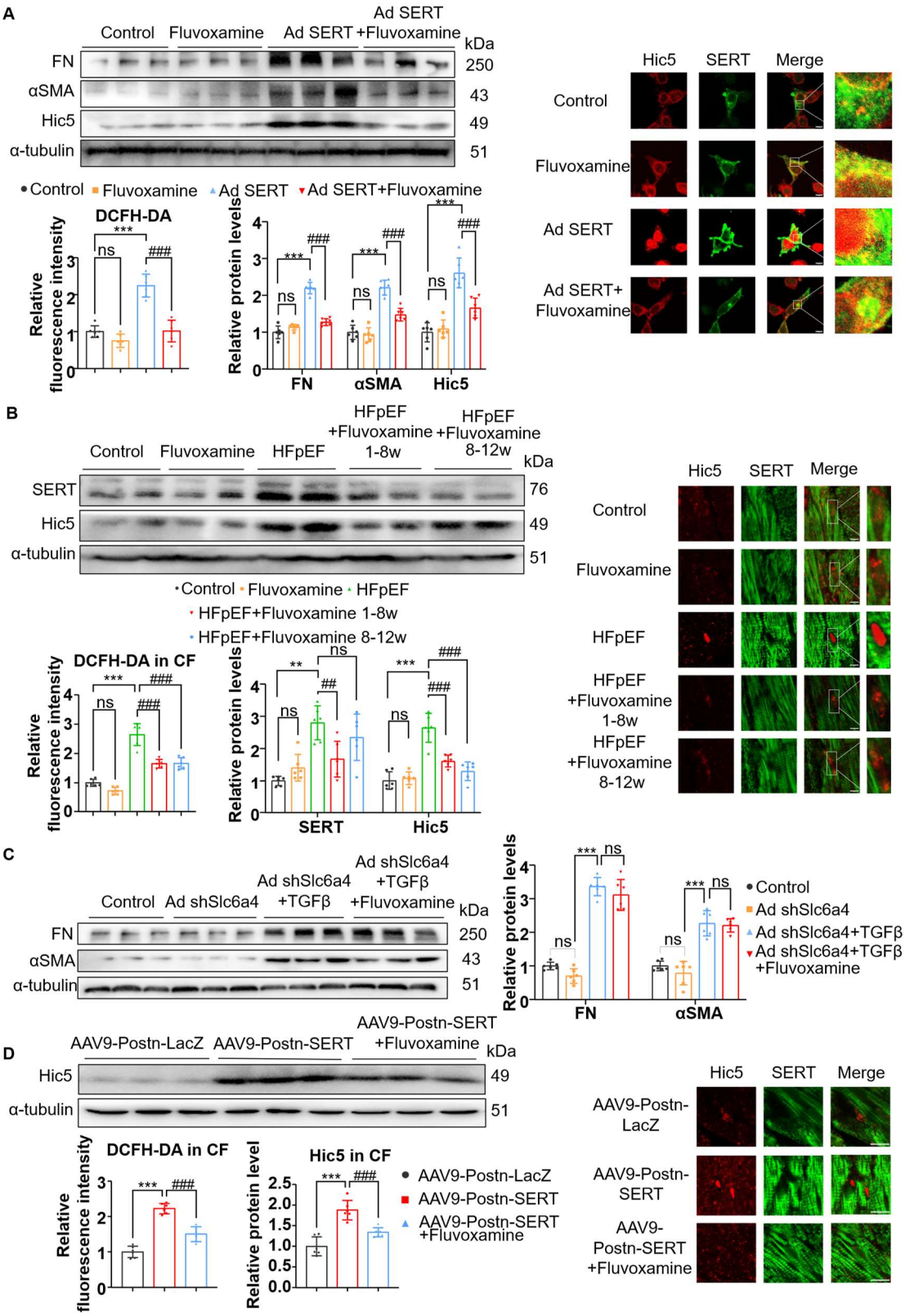
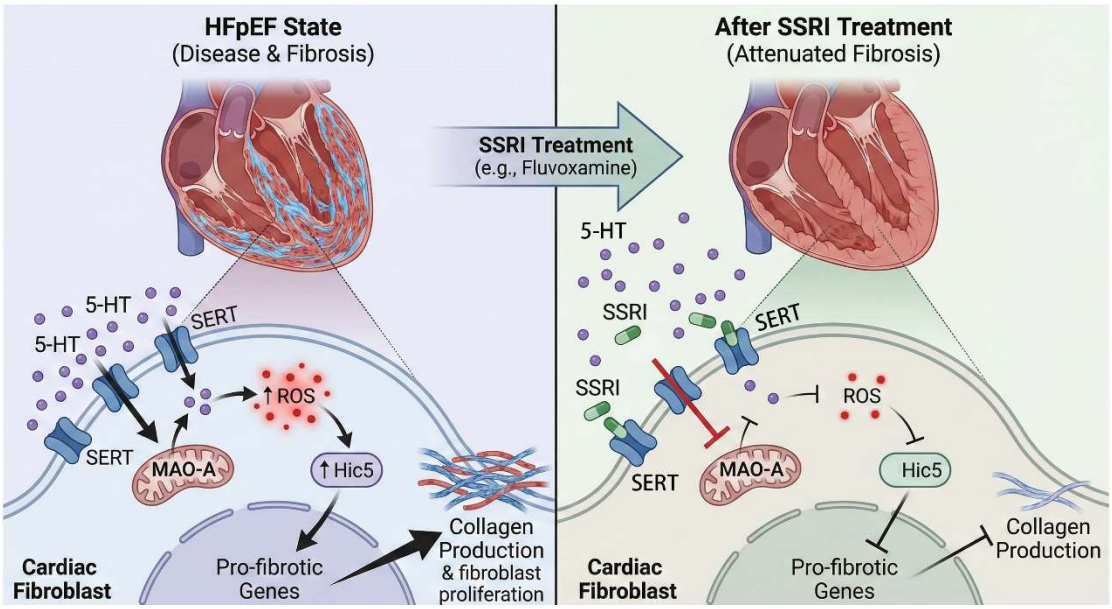


Figure 8. The SSRI fluvoxamine inhibits SERT overexpression-induced increases in ROS and Hic5 levels in vitro and in vivo. A, Left, Measurement of intracellular

ROS levels using DCFH-DA fluorescence intensity, representative Western blot and average data showing protein levels of FN, αSMA and Hic5 in cardiac fibroblasts transfected with Ad-SERT or Ad-LacZ and treated with or without 10μM Fluvoxamine. n = 6 independent experiments. Statistical significance was assessed by One way ANOVA analysis followed by Bonferroni's post hoc test. **Right,** immunofluorescence staining showing SERT and Hic5 protein level in cardiac fibroblasts transfected with Ad-SERT or Ad-LacZ and treated with or without 10μM Fluvoxamine. Scale bar = 10 μm. **B, Left,** Measurement of intracellular ROS levels using DCFH-DA fluorescence intensity, representative Western blot and average data showing protein levels of SERT and Hic5 in isolated cardiac fibroblasts from HFpEF mice treated with fluvoxamine preventively (weeks 1-8) or therapeutically (weeks 8-12). Cardiac fibroblasts were isolated from n = 6 mice per group. Statistical significance was assessed by One way ANOVA analysis followed by Bonferroni's post hoc test. **Right,** immunofluorescence staining showing SERT and Hic5 protein level in heart tissues. Scale bar = 5 μm. **C,** Representative Western blot and average data showing protein levels of FN, αSMA and Hic5 in cardiac fibroblasts transfected with Ad-SERT/Ad-LacZ and Ad-shTgfb1i1/Ad-scRNA. n = 6 independent experiments. Statistical significance was assessed by One way ANOVA analysis followed by Bonferroni's post hoc test. **D, Left,** Measurement of intracellular ROS levels, representative Western blot and average data showing protein levels of Hic5 in isolated cardiac fibroblasts from mice injecting AAV9 driven by the Postn promoter (AAV9-Postn-SERT) /AAV9-Postn-LacZ and 10 mg/kg/d Fluvoxamine. n = 6 mice per group. Statistical significance was assessed by One way ANOVA

analysis followed by Bonferroni's post hoc test. **Right,** immunofluorescence staining showing SERT and Hic5 protein level in heart tissues. Scale bar = 10 μm.



SSRIs inhibit fibroblast activation via suppression of the SERT/ROS/Hic5 signaling axis in HFpEF. In HFpEF state, SERT is upregulated in cardiac fibroblasts, then SERT-mediated 5-HT uptake promotes its degradation by monoamine oxidase A (MAO-A), which generates ROS. ROS subsequently drive the transcriptional upregulation of the co-regulator Hic5, thereby activating pro-fibrotic cascades that leads to collagen production and diastolic dysfunction. Therapeutic administration of SSRIs (e.g., fluvoxamine) specifically inhibits SERT, blocking this maladaptive 5-HT/MAO-A/ROS/Hic5 signaling cascade and reducing fibrosis in HFpEF.

1051 **Tables**

1052 Table 1. The baseline characteristic of in hospital HFpEF patients

	Overall populations (n = 730)	**HFpEF without SSRIs（n = 619）**	**HFpEF with SSRIs（n = 111）**	***P*-value**
Gender, Female(%)	401 (54.93)	327 (52.83)	74 (66.67)	**0.009***
Age, y	70.00 (62.00, 77.00)	70.00 (63.00, 77.50)	71.00 (60.00, 77.00)	0.689
BMI, kg/m^2	25.27 (23.23, 27.67)	25.39 (23.52, 27.73)	24.57 (22.40, 26.83)	**0.001***
Comorbidity				
Hypertension, n(%)	193 (26.44)	165 (26.66)	28 (25.23)	0.843
Diabetes, n(%)	462 (63.29)	385 (62.20)	77 (69.37)	0.181
Hyperlipidemia, n(%)	562 (76.99)	489 (79.00)	73 (65.77)	**0.003***
CKD, n(%)	227 (31.10)	181 (29.24)	46 (41.44)	**0.014***
AF, n(%)	529 (72.47)	446 (72.05)	83 (74.77)	0.634
CHD, n(%)	337 (46.16)	274 (44.26)	63 (56.76)	**0.020***
Medication				
ACEI/ARB, n(%)	377 (51.64)	313 (50.57)	64 (57.66)	0.203
SGLT2i, n(%)	471 (64.52)	383 (61.87)	88 (79.28)	**0.001***
β blockers, n(%)	299 (40.96)	249 (40.23)	50 (45.05)	0.398
Statins, n(%)	190 (26.03)	158 (25.53)	32 (28.83)	0.540

1053 BMI, Body Mass Index; ACEI/ARB, Angiotensin-Converting Enzyme

Inhibitor/Angiotensin II Receptor Blocker; SGLT2i, Sodium-Glucose Cotransporter 2 Inhibitor.

Table 2. Association between the SSRIs usage and cardiac function indicators (Gamma GLM model)

	Model	Mean Ratio [95% CI]	*P*
BNP	Model 1	0.66 (0.511 - 0.854)	**0.0016***
	Model 2	0.655 (0.505 - 0.849)	**0.0015***
	Model 3	0.664 (0.532 - 0.828)	**0.0003***
E/e'	Model 1	0.919 (0.843 - 1.003)	0.0575
	Model 2	0.92 (0.841 - 1.006)	0.0662
	Model 3	0.923 (0.857 - 0.994)	**0.0352***
E/A	Model 1	0.884 (0.806 - 0.97)	**0.0093***
	Model 2	0.886 (0.809 - 0.972)	**0.0102***
	Model 3	0.883 (0.813 - 0.958)	**0.0031***
LAD	Model 1	0.996 (0.964 - 1.03)	0.826
	Model 2	1.000 (0.969 - 1.032)	0.9887
	Model 3	1.008 (0.983 - 1.033)	0.632
LVMI	Model 1	0.918 (0.87 - 0.969)	**0.002***
	Model 2	0.925 (0.878 - 0.975)	**0.0035***
	Model 3	0.931 (0.884 - 0.981)	**0.0076***
RWT	Model 1	1.002 (0.969 - 1.037)	0.892
	Model 2	1.000(0.966 - 1.035)	0.9993
	Model 3	0.999 (0.966 - 1.033)	0.9712

BNP, B-type Natriuretic Peptide; LAD, Left Atrial Diameter; LVMI, Left Ventricular Mass Index; LVPWd, Left Ventricular Posterior Wall thickness in diastole; RWT, Relative Wall Thickness.

1062 Table 3. The baseline characteristic of in MIMIC HFpEF patients

	Overall populations (n=1089)	**HFpEF without SSRIs （n=909）**	**HFpEF with SSRIs （n=180）**	***P*-value**
Gender, Female,n(%)	567 (52.1)	455 (50.1)	112 (62.2)	**0.003***
Age, y	74.00 (65.00, 81.00)	74.00 (65.00, 82.00)	72.00 (64.00, 79.00]	**0.047***
BMI, kg/m²	32.40 (27.50, 39.30)	32.10 (27.30, 38.80)	34.70 (28.87, 42.27)	**0.001***
Comorbidity				
Hypertension, n(%)	182 (16.7)	148 (16.3)	34 (18.9)	0.383
Diabetes, n(%)	528 (48.5)	443 (48.7)	85 (47.2)	0.744
Hyperlipidemia, n(%)	627 (57.6)	523 (57.5)	104 (57.8)	>0.999
CKD, n(%)	372 (34.2)	317 (34.9)	55 (30.6)	0.302
AF, n(%)	505 (46.4)	430 (47.3)	75 (41.7)	0.191
CHD, n(%)	543 (49.9)	463 (50.9)	80 (44.4)	0.121
Medication				
ACEI/ARB, n(%)	469 (43.1)	395 (43.5)	74 (41.1)	0.621
β blockers, n(%)	788 (72.4)	655 (72.1)	133 (73.9)	0.649
Statins, n(%)	778 (71.4)	645 (71.0)	133 (73.9)	0.47
Clinical score				
SOFA score-total	3.00 (1.00, 5.00)	3.00 (1.00, 6.00)	2.50 (1.00, 5.00)	**0.006***
SOFA score-	1.00 (0.00, 1.00)	1.00 (0.00,	1.00 (0.00,	0.133

cardiovascular		1.00)	1.00)

BMI, Body Mass Index; ACEI/ARB, Angiotensin-Converting Enzyme Inhibitor/Angiotensin II Receptor Blocker; SOFA score, Sequential Organ Failure Assessment score on admission.

Table 4. Association between the SSRIs usage and outcome measures in the MIMIC-IV database (Gamma GLM model)

	Model	**Mean Ratio [95% CI]**	***P***
SOFA score-total	Model 1	0.753 (0.677 - 0.838)	**< 0.001***
	Model 2	0.824 (0.731 - 0.929)	**0.0016***
	Model 3	0.818 (0.746 - 0.898)	**< 0.001***
SOFA score-cardiovascular	Model 1	0.965 (0.841 - 1.107)	0.6111
	Model 2	0.992 (0.861 - 1.143)	0.9073
	Model 3	1.010 (0.894 - 1.141)	0.8753
All-cause mortality	Model 1	0.514 (0.155 - 1.707)	0.2772
	Model 2	0.577 (0.170 - 1.959)	0.3783
	Model 3	0.627 (0.181 - 2.168)	0.4605

SOFA score, Sequential Organ Failure Assessment score at discharge.

Supplementary Files

This is a list of supplementary files associated with this preprint. Click to download.

- supplement1019.pdf